6 GHZ DIRECT MODULATION 20 KM REACH ANALOG OPTICAL TRANSCEIVER DESIGN

XIANG LING DAI

A Thesis
in
The Department
of
Electrical and Computer Engineering

Presented in Partial Fulfillment of the Requirements
for the Degree of Master of Applied Science
(Electrical & Computer Engineering) at
Concordia University
Montreal, Quebec, Canada

May 2012

CONCORDIA UNIVERSITY
SCHOOL OF GRADUATE STUDIES

This is to certify that the thesis prepared

By: Xiang Ling Dai

Entitled: "6 GHz Direct Modulation 20 Km Reach Analog Optical Transceiver Design"

and submitted in partial fulfillment of the requirements for the degree of

Master of Applied Science

Complies with the regulations of this University and meets the accepted standards with respect to originality and quality.

Signed by the final examining committee:

_____ Chair
Dr. S. Williamson

_____ Examiner, External
Dr. A. Ben Hamza (CIISE) To the Program

_____ Examiner
Dr. D. Qiu

_____ Supervisor
Dr. X. Zhang

Approved by: _____
Dr. W. E. Lynch, Chair
Department of Electrical and Computer Engineering

_____20_____ _____
Dr. Robin A. L. Drew
Dean, Faculty of Engineering and
Computer Science

ABSTRACT

6 GHz Direct Modulation 20 Km Reach Analog Optical Transceiver Design

Xiang Ling Dai

Optical links for the transmission of analog signals have continued to expand thanks to its simplicity, low loss, large bandwidth, low cost, and immunity to electromagnetic interference from external RF sources. However, due to the lack of economic analog transceiver which has the highest operation frequency between 3 to 10 GHz in current market, the applications within this band need to use the 10 GHz transceiver product, which inevitably complicates the system design and increases the associated cost.

In this thesis, a cost effective 6 GHz 20 Km reach optical analog transceiver is proposed, designed, and experimentally demonstrated. Theoretical analysis and design of the system is performed through the power budget analysis, bandwidth budget analysis, noise analysis, linearity analysis, and economic consideration. Several criteria for choosing components are proposed accordingly. An OptiSystem RoF application simulation is conducted to verify the analysis results. After choosing components and fabricating the circuit, we perform DC and AC test for both transmitter and receiver, link S parameter measurement, SFDR measurement by two tone test, and 20 Km fiber transmission UWB OFDM single channel test and multi-channel test, the result demonstrates that the proposed transceiver has more than 6 GHz 3-dB gain bandwidth with -10 dB link gain and very good match at its input and output impedances, 31 dB link noise figure, -9 dBm

output P1dB, 10 dBm OIP3 and 102 dB SFDR, and it's an ideal option for OFDM UWB RoF systems.

In RoF system, a post amplifier is almost following the optical receiver. It boosts the output RF signal power to facilitate the further use of the signal. A proposed 6 GHz 30 dB gain 1 Watt power amplifier is also designed, fabricated, and experimentally demonstrated within this thesis.

Finally, the further search for better components to improve the transceiver performance, the size optimization of the transceiver, and the design of an adaptor for LC receptacle and LC connector are proposed as future research topics.

ACKNOWLEDGEMENTS

I would like to take this opportunity to express my sincere appreciation to my supervisor Dr. Xiu Pu Zhang for his guidance, patience, trust, and financial support for me to finish this thesis. Under his supervision, I have undertaken an interesting study in the field of microwave photonic circuit design, and I have also gained experience in the Advanced Photonic Systems Lab. Without his trust and inspiration I couldn't have overwhelmed the different obstacles on my way of studying the circuit design, fabrication, and experiment. His diligent and serious attitude towards the research always encourages me to pursue the best along the way in my research.

I would also like to express my appreciation to Dr. Bouchaib Hraimel (Lab Manager in Advanced Photonic System Lab, Concordia University) for his insightful guidance, advice and encouragement during the whole project.

Also I would like to thank Mr. Ttaian Antonescu with Poly-Grames Research Center (Centre de Recherche en Électronique Radio fréquence (CREER)) for his technical assistance and suggestion in PCB fabrication of the prototype circuit and thank Dr. Yousef R. Shayan for providing the RF sources.

I am very grateful to my wife, Xiao Chun Jia; many thanks for her continuous love and support. Without her understanding and support, this work would never be done.

TABLE OF CONTENT

LIST OF FIGURES

LIST OF TABLES

LIST OF ACRONYMS

AM	Amplitude Modulation
APD	Avalanche photo-detector
AWG	Arbitrary waveform generator
BJT	Bipolar junction transistor
CATV	Cable television
CNR	Carrier-to-noise ratio
CW	Continuous wave
DCM	Dual carrier modulation
DFB	Distributed-feedback laser
DSO	High speed real time oscilloscope
E/O	Electrical-to-optical
EAM	Electro-absorption modulator
EVM	Error vector magnitude
FP	Fabry-Perot laser
HD	Harmonic distortion
IMD	Inter-modulation distortion
LD	Laser diode
LED	Light emitting diode
LNA	Low noise amplifier
MLM	Multiple-longitudinal mode
MMF	Multi Modal Fiber

MZM	Mach-Zehnder modulator
O/E	Optical-to-electrical
OFDM	Orthogonal frequency-division multiplexing
PCB	Printed Circuit Board
PD	Photo diode
PIN	p-i-n photo-detector
RF	Radio frequency
RIN	Relative intensity noise
RoF	Radio over Fiber
ROSA	Receive Optical Sub-Assembly
SFDR	Spurious Free Dynamic Range
SLM	Single-longitudinal mode
SMF	Single modal fiber
SNR	Signal-to-noise ratio
TIA	Trans-impedance amplifier
TO-Can	Transistor outline-can
TOSA	Transmit Optical Sub-Assembly
UWB	Ultra-wideband
VCSEL	Vertical-Cavity Surface-Emitting Laser
VRA	Variable RF attenuator

CHAPTER 1 INTRODUCTION

1.1 Analog Optical System

In telecommunication networks, there are many applications which transmit information in analog form instead of preliminarily converting it to a digital format and ultimately converting it back. Among the examples of these applications are microwave-multiplexed signals, subscriber-loop applications, video distribution, antenna remoting, and radar signal processing [1]. Ever since the first commercial analog optical links were introduced in cable television (CATV) distribution two decades ago, the application of optical links for the transmission of analog signals has experienced a continuing expansion because of the simplified system, the low attenuation, the large bandwidth, the low cost, and also the potential it promises [2]. In recent years, Radio over Fiber (RoF) has become increasingly popular in analog optical links [3]. Briefly, RoF represents a technology enabling the modulation of light via radio signals as well as the signal transmission over an optical fiber link so as to facilitate wireless access. By virtue of RoF solutions, high-performance fiber optic links are able to natively transport radio frequency (RF) signals over a wide range of bands including 1 kHz, L-band, S-band, C-band, Ku-band, and Ka-band. The effective long-distance travel of these analog microwave signals can be attributed to the fiber's low insertion loss (as the link distances range from a few hundred meters to fifty kilometers). In addition, optical fiber is superior to coaxial cable due to its light weight and immunity to electromagnetic interference from external RF sources. Recently, the market sees the lowering cost in optical components,

and accompanied with it is the phenomenon that RoF systems have gained extensive research interest and gradually spread into the telecommunication industry [4-7].

A basic RoF configuration as shown in Fig. 1.1 consists of a two-way interface that contains an electrical-to-optical (E/O) transmitter and optical-to-electrical (O/E) receiver which connects the central base station transmitters and receivers to a pair of single mode optical fiber [8]. At the other end of the fiber a similar O/E receiver and E/O transmitter are used to convert optical signals to and from an antenna.

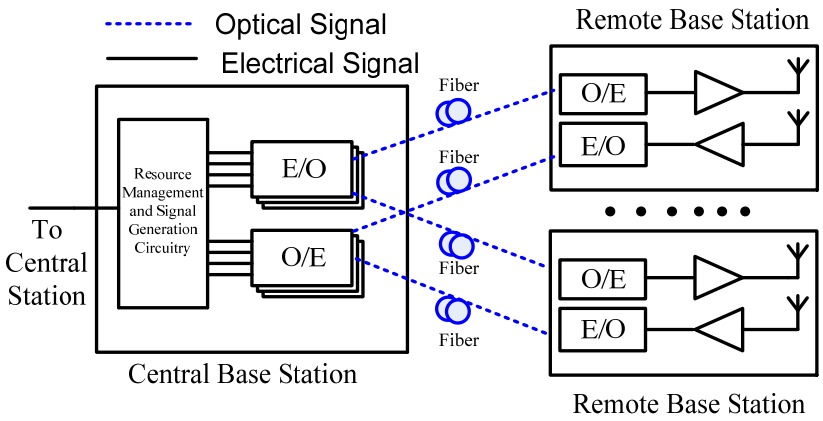

Figure 1.1 Radio over Fiber System [9]

1.2 Motivation and Review of Technologies

Optical analog transceiver (transmitter and receiver) is the core component of the RoF system, which links the optical domain to the electrical domain. It converts the signal from electrical to optical and launches it into the optical fiber. It also receives the optical signal from optical fiber and converts it to electrical signal.

In the current market, there are plenty of analog optical transmitters and receivers. If we classify them by the highest operation frequency, there will be two groups, one of which is up to 3 GHz and lower, and another one is minimum 10 GHz and higher. There is no product with the highest operation frequency between these two. This can be shown in Table 1-1, a list of all the microwave fiber link analog transmitters of Emcore Inc. a leading provider of compound semiconductor-based components and subsystems for the fiber optics markets. Moreover, the costs of these two group products have a significant difference: the low frequency products are cheaper and the high frequency products are much more expensive. This means that if one system just needs the high operation frequency between 3 to 10 GHz, one has to use the expensive transmitter and thus the system cost is high. In the following, we will briefly explain why there is such a big cost difference between these two groups.

Table 1-1 Emcore Inc. microwave fiber link transmitter list

Product No.	Operation Frequency Range
OTS-1RefT	Transmitter, 1MHz - 20MHz
SITU2011	Transmitter, 1MHz – 3GHz
OTS-1LDT	Transmitter, 50MHz – 3GHz
3541A	Transmitter, 1MHz – 10GHz
3541B	Transmitter, 1MHz – 13GHz
5021T-C	Transmitter, 1MHz – 13GHz
3541C	Transmitter, 1MHz – 15GHz
3541C-E05	Transmitter, 1MHz – 18GHz
5021T-D	Transmitter, 1MHz – 18GHz
SITU3000	Transmitter, 50MHz – 18GHz
OTS-2T/S5-0518-10-YY-ZZ	Transmitter, 50MHz - 18GHz
OTS-2T/K5-0518-10-YY-ZZ	Transmitter, 50MHz – 18GHz
5021T-E	Transmitter, 1MHz – 22GHz
OTS-2T/K5-0522-XX-YY-ZZ	Transmitter, 50MHz – 22GHz
SITU3040	Transmitter, 50MHz – 40GHz

OTS-2T/K5-0540-XX-YY-ZZ	Transmitter, 50MHz – 40GHz

As for an optical transceiver, when compared with the wide bandwidth of the photo-detector, its frequency range mainly depends on the modulation frequency of the light source [12]. Basically, there are two alternative ways to generate a modulated optical signal, which are direct modulation and external modulation. Figure 1.2 illustrates these two alternatives.

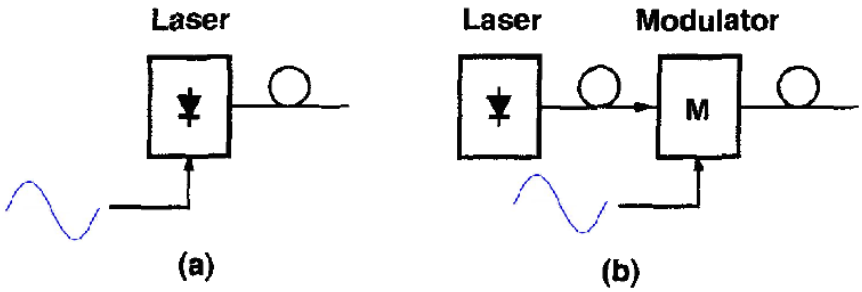

Figure 1.2 Optical Transmitters: (a) direct modulation vs. (b) external modulation. [10]

In Figure 1.2(a), the optical signal is obtained by using the signal to directly modulate the light source current (which is the summation of signal current and the bias current); this method is known as direct modulation. The output optical signal is shown in Figure 1.3. In Figure 1.2(b), where the light source is always on with constant output power (the light source current is just the bias current), a so-called continuous wave (CW) light source and a subsequent optical modulator are used to modulate the light with the electrical signal. This method is known as external modulation.

For the direct modulation, the operation frequency is just the light source's modulation frequency, and it is completely decided by the light source fabrication, which can be

given by [11] as $f_{3dB} \approx \sqrt{\frac{3G_N P_b}{4\pi^2 \tau_P}}$, where G_N is a constant for a given light source, P_b is the steady-state value at the bias current, and τ_P is referred to as the photo lifetime. Therefore, for a built light source at fixed bias current, its bandwidth cannot be changed externally. The aforesaid low frequency group products all use direct modulation, and the highest 3 dB bandwidth of most current market products is around 3GHz, that's why they operate at 3 GHz and below.

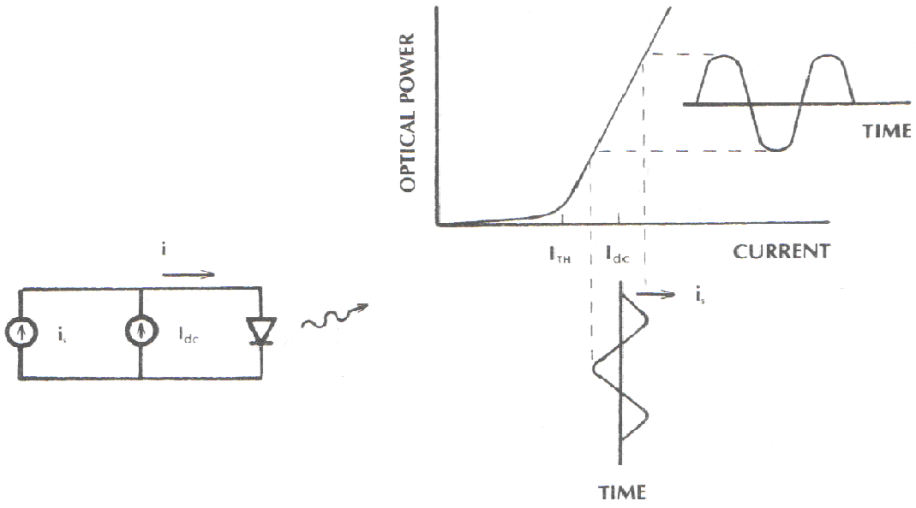

Figure 1.3 Direct modulation of a laser diode [12]

On the contrary, the high frequency group products all use external modulation. Since the light source provides constant optic power, the bandwidth is decided by the optical modulator. Two types of optical modulators are commonly used in communication systems: the electro-absorption modulator (EAM) and the Mach-Zehnder modulator (MZM).

The EAM sandwiches an active semiconductor region between a p-doped and n-doped layers, forming a p-n junction. The EAM works on the principle that an increasing electric field can decrease the effective band-gap of a semiconductor. Without bias voltage across the p-n junction, the band-gap of active region is wide enough, thus the light can pass without absorption as the photon energy is less than the gap energy. However, when a sufficient reverse bias is applied, the effective band-gap is reduced and thus the output light power is reduced due to absorption. The switching curve, which is the relationship between the optical output power P_{out} and the applied reverse voltage V_M, is shown in Figure 1.5. An EAM always follows a CW distributed-feedback laser (DFB), as shown in Figure 1.4. Both devices can be integrated on the same substrate, and operation beyond 40 GHz is available for EAM [13].

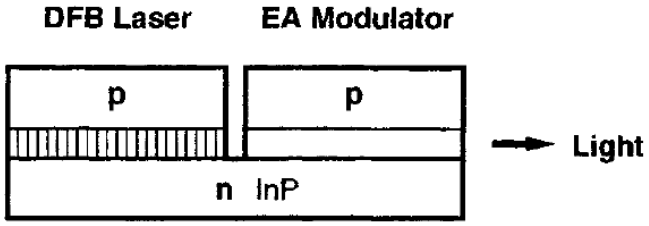

Figure 1.4 Integrated laser and EAM (schematically). [13]

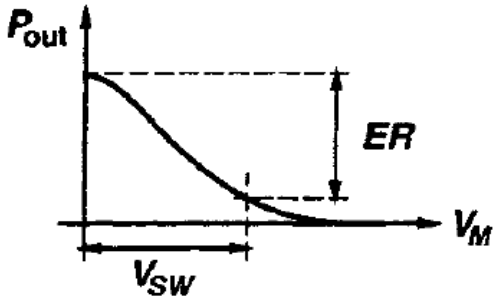

Figure 1.5 Switching curve of an EAM [13]

MZM modulator works on the principle of electro-optic effect, which means that with the presence of an electric field, the refractive index of some materials such as lithium niobate (LiNbO3), some semiconductors, and some polymers will be changed. Figure 1.6 (left) shows the top view of an MZM modulator. The incoming optical signal is split equally and is sent to two different optical paths. After a short distance, the two paths recombine, thus the two optical signals interfere with each other. By way of changing the electrical field across the optical wave path, the refractive index and then the phase of the two optical signals are changed accordingly. The output optic power, which is the combination of these two optical signals, will vary with the electrical field applied. Figure 1.6 (right) shows a cut view through an MZM modulator based on lithium niobate. The switching curve of an MZM is shown in Figure 1.7. Operation beyond 40 GHz is also available for MZM [13].

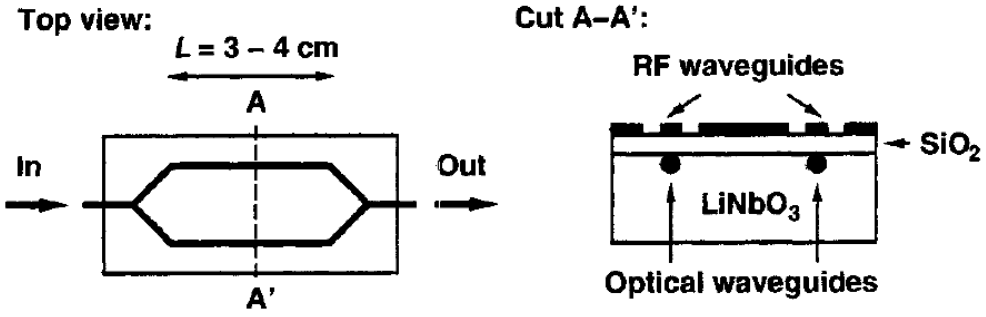

Figure 1.6 Dual-drive MZM based on LiNbO3 (schematically). [13]

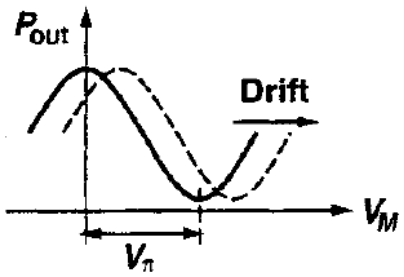

Figure 1.7 Switching curve of a MZM. [13]

The 10 GHz and more high frequency group products all use external modulation. Compared with the direct modulation, except the additional structure described above, the external modulators still suffer nonlinearity and high insertion loss which need extra linearization circuits and optic amplifier. All these factors entail the cost of the external modulation transmitter higher than that of the direct modulation one.

As the fabrication technology evolves, the light sources around 6 GHz modulation bandwidth makes their appearance on the market in recent year, which enables the designing of an economic optical transceiver (direct modulation) with operation frequency range great than 3 GHz. This can greatly reduce the cost of most optical applications within this frequency band, and thus implies huge potential for economic benefits. It is based on this consideration that the thesis proposes and presents a 6 GHz direct modulation 20 km reach analog optical transceiver design.

1.3 Thesis Scope and Contributions

The focus of this research work is on designing a simple and economical 6 GHz direct modulation with 20 km reach analog optical transceiver. The theoretical analysis and

calculation, software simulation, product fabrication, and experimental verification are presented in detail.

The main contribution of this thesis is to design, implement and experimentally demonstrate a cost-effective product, namely a 6 GHz direct modulation 20 km reach analog optical transceiver, the first of its kind in the field of optical communication.

1.4 Thesis Outline

The rest of the thesis is organized as follows:

Chapter 2: theoretically analyze and calculate all the considerations of the product design, and provide components choosing criterions.

Chapter 3: Conduct OptiSystem simulation to verify the analyses in Chapter 2.

Chapter 4: Choose all the components needed, fabricate the overall product.

Chapter 5: Experimental demonstration of the fabricated product.

Chapter 6: Conclude the thesis and make suggestions for the future work.

CHAPTER 2 THEORETICAL ANALISIS

Having taken into consideration all the functions of an optical transceiver, we design its block diagram as shown in Figure 2.1. All blocks inside the dashed box is the transceiver. The RF signal after linearization through a RF interface gets into the system and directly modulates the light source to generate optical signal, and then launches the optic signal into the optical fiber through an optical interface. On the other side, the optical signal from the optical fiber inputs to the photo-detector through an optical interface, and the photo-detector converts the optical signal to electrical signal and transmits through a RF interface to a post amplifier for further use. The Monitor & Control is responsible for monitoring and controlling the whole system.

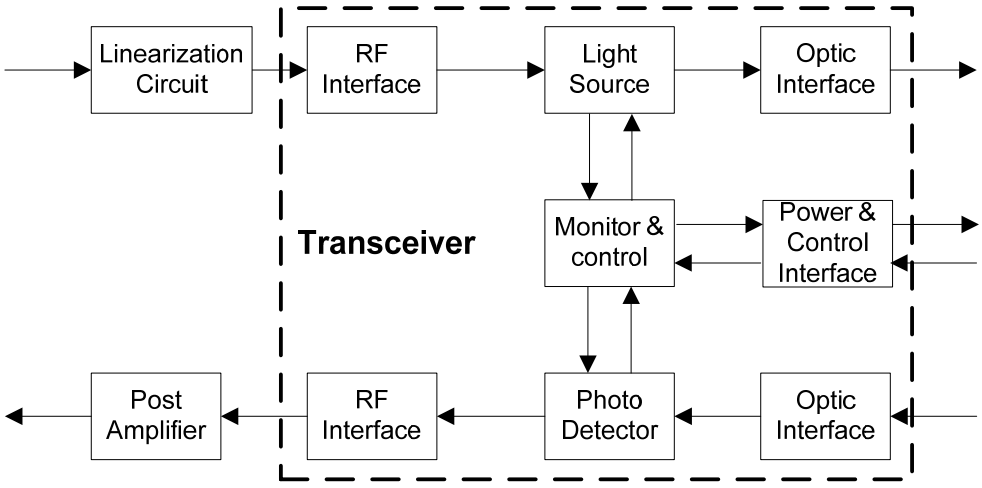

Figure 2.1 Transceiver block diagram

We mentioned the linearization circuit and post amplifier in the block diagram because in the RoF system, these two circuits are always used with the transceiver. The linearization circuits can significantly improve the transmitter's linearity, and the post amplifier will

boost the receiver output signal power to facilitate the further use of the signal. A 6GHz 30 dB gain 1 Watt power amplifier has been designed, fabricated, and tested already, please see Appendix A for detail. The linearization circuit will be discussed in Section 2.1.4. In the rest of this section, we will present the detail analysis and design for the transceiver.

2.1 Light Source and Photo-Detector

In the fiber system, the information is carried via optic beams generated by light sources. The role of the photo-detector is to convert the optical signal back into electrical form and recover the data transmitted through the light-wave system. The choice of the light source and photo-detector is dependent on the optical power needed, the bandwidth desired, the maximum noise allowed, and the linearity performance.

2.1.1 Power Budget

To perform a power budget analysis is to make sure that there will be enough optic power reaching the photo-detector so that the system will output qualified signal. The minimum power needed by the photo-detector is called as photo-detector sensitivity. By writing the power level in dBm, the relationship between the minimum output power generated by light source and the sensitivity of the photo-detector can be expressed by the following formula,

$$P_{out-\min}(dBm) = P_{PD-sensitivity}(dBm) + P_{total-loss}(dB) + P_{margin}$$

where $P_{PD-sensitivity}$ is the photo-detector sensitivity; $P_{total-loss}(dB)$ includes coupling loss, connector loss, splice loss, and fiber attenuation; P_{margin} is the power margin which is chosen around 3 dB here. We assume there are 3 dB source-fiber coupling loss, two connectors of 1 dB loss each, 10 splices of 0.1 dB loss each, and 20 km reach with 0.35 dB attenuation per km fiber. Then the formula became,

$$P_{out-\min}(dBm) = P_{PD-sensitivity}(dBm) + 3dB + 1dB \times 2 + 0.1dB \times 10 + 0.35dB \times 20 + 3dB$$

$$P_{out-\min}(dBm) = P_{PD-sensitivity}(dBm) + 16dB$$

which means

$$P_{laser-out}(dBm) \geq P_{PD-sensitivity}(dBm) + 16dB$$

This is the relationship between the light source output and the photo-detector sensitivity and will be used as one criterion to choose light source and photo-detector.

2.1.2 Bandwidth Budget

In order to assure sufficient bandwidth for the system, the bandwidth restrictions contingent on the combining the source, fiber, and detector will be analyzed. Since the rise time of these components will be given in most cases, we will do the analysis in terms of rise time. The relationship between the 3-dB bandwidth and the system rise time is as following [14]

$$f_{3-dB} = \frac{0.35}{t_S}$$

where t_s is the overall system rise time. Based on the required bandwidth, 6 GHz (plus 10% margin), the system rise time should be

$$t_S < \frac{0.35}{f_{3-dB}} = \frac{0.35}{6.6 \times 10^9} = 53ps$$

The system rise time t_S includes light source rise time t_{LS}, fiber rise tine t_F, and photo-detector rise time t_{PD}, and they are approximately related by [15]

$$t_S^2 = t_{LS}^2 + t_F^2 + t_{PD}^2$$

The total fiber rise time can be found from [16]

$$t_F^2 = t_{dis}^2 + t_{\text{mod}}^2$$

where t_{dis} is the equivalent rise time due to the fiber dispersion, and t_{mod} is the equivalent rise time due to the multimode dispersion. The fiber dispersion equivalent rise time can be found from [17]

$$t_{dis} = (D_M + D_W)L\Delta\lambda$$

where D_M is the fiber material dispersion, D_W is the fiber waveguide dispersion, L is the fiber length, and $\Delta\lambda$ is the light source spectral width. Then the overall system rise time becomes

$$t_S = \sqrt{t_{LS}^2 + t_{PD}^2 + ((D_M + D_W)L\Delta\lambda)^2 + t_{\text{mod}}^2} < 53ps$$

For a multimodal fiber, $t_{\text{mod}} \approx \frac{NA^2}{2cn_1}$ [18], where NA is the numerical aperture of the fiber, n_1 is the refraction index of the fiber core, and c is the speed of light in vacuum. By using typical value of NA and n_1, one can find that t_{mod} is at the level of nanoseconds, which is not acceptable here, so single modal fiber (SMF) has to be used to get rid of the effect of the multimode dispersion (let $t_{\text{mod}} = 0$). Figure 2.2 illustrates the total dispersion D and relative contributions of material dispersion D_M and waveguide dispersion D_W for a conventional single-mode fiber. λ_{ZD} is referred to as the zero-dispersion wavelength ($D = D_m + D_W = 0$). One can see that for this single-mode fiber, the total dispersion is zero near 1310 nm. To maximize the bandwidth, we will choose 1310 nm as our system wavelength to minimize the fiber dispersion effects. By using some special fibers, such as dispersion-shifted fibers or dispersion-compensating fibers, it also can achieve very small fiber rise time, but this will simultaneously increase the cost. Based on previous assumptions, one can get

$$t_S = \sqrt{t_{LS}^2 + t_{PD}^2} < 53ps$$

Assume $t_{LS} = t_{PD} = t_{rise}$, the result is $t_{rise} < 37ps$ for both light source and photo-detector.

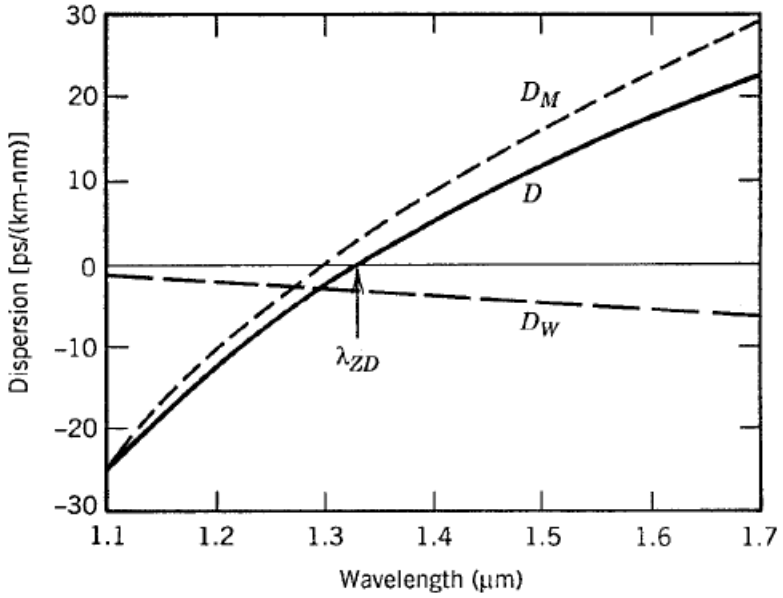

Figure 2.2 Total dispersion D and relative contributions of material dispersion D_M and waveguide dispersion D_W for a conventional single-mode fiber. [19]

2.1.3 Noise Analysis

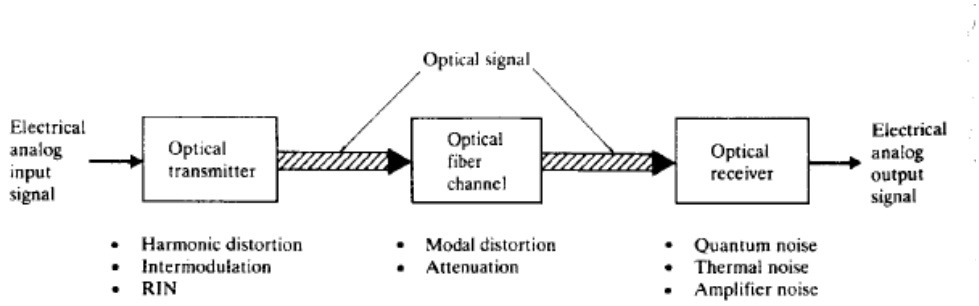

Figure 2.3 Basic elements of an analog link and the major noise contributions. [20]

Figure 2.3 illustrates the basic elements of an analog link and the major noise contributions. Minor noise sources are not critical and will be ignored here. In this section,

we investigate the major sources of noise and how to compute the noise power. A signal's quality, measured by the signal-to-noise ratio, can then be calculated.

2.1.3.1 Transmitter Noise

There are several modulation techniques to transmit the analog signal, such as direct intensity modulation in the base band or the translation of the base band signal into an electrical subcarrier prior to intensity modulation of the source. No matter which method is implemented, there will be several noise sources that one should pay careful attention to. These include harmonic distortions (HD), inter-modulation distortion (IMD) products, and relative intensity noise (RIN) in the laser.

We will use sine wave as the input signal to introduce the harmonic distortion and inter-modulation distortion as following. When the input is a single signal, $x(t) = A\sin(2\pi ft)$ with amplitude A and frequency f, as we know, the output signal contains harmonic components at f, $2f$, $3f$, and so forth. The components except at f will contribute distortion to the signal, and is called harmonic distortions. When the input signal to the linear channel is not a single sine wave, except the harmonic distortions, there will be also inter-modulation distortion occurrence. Assume $x(t) = A(\sin(2\pi f_1 t) + \sin(2\pi f_2 t))$,then the output will contain two second-order inter-modulation products at $\left| f_1 + f_2 \right|$ and $\left| f_1 - f_2 \right|$, four third-order inter-modulation products at $\left| 2f_1 + f_2 \right|$,$\left| 2f_1 - f_2 \right|$,$\left| 2f_2 + f_1 \right|$,and $\left| 2f_2 - f_1 \right|$, and so on.

For a wideband system, all the harmonic distortion and inter-modulation distortion within the operation band should be taken into account to the system's linearity. Harmonic

distortions and inter-modulation distortion are not random. Instead, they appear at certain frequency. At low power level, compare with the RIN noise, the power of these distortions are very low, thus a direct modulated light source will have very good linearity. Moreover, there will be a linearization circuit to minimize this effect, so we ignore this part and consider the RIN noise only. The output of a semiconductor laser is not constant even when the laser is biased at a constant current. It exhibits fluctuations in its intensity, phase, and frequency. Spontaneous emission and electron-hole recombination are the two fundamental noise mechanisms, where the spontaneous emission is dominant [21]. Each spontaneously emitted photon is random in amplitude and phase, and high rate of this random manner will make the emitted light (established by stimulated emission) exhibit fluctuations on both intensity and phase. When a semiconductor lasers are operated at a constant current, the intensity fluctuations will decrease the signal-to-noise ratio (SNR) and is called RIN noise, whereas phase fluctuations will increase the light spectral line-width. The RIN noise can be calculated approximately by [20]

$$\overline{i_{NL}^2} = RIN(\rho P)^2 \Delta f$$

where $\overline{i_{NL}^2}$ is the mean squared value of the laser noise current, RIN is the relative intensity noise parameter of the laser (is always given for a fabricated laser), ρ is the photo-detector responsivity, P is the average output power, and Δf is the electrical bandwidth of the photo-detector. This equation shows that the RIN noise is proportional to the generated optic power.

2.1.3.2 Optical Fiber Noise

In relation to the fiber-optic element shown in Figure 2.3, one must take into account the frequency dependence of amplitude, phase, and group delay in the fiber. Thus the fiber should have a flat amplitude and group-delay response within the pass-band required to send the signal free of linear distortion. Fortunately, there are good single modal fibers available in the current market, which will generate negligible noise if compared with the source and detector noise. So we assume an ideal single modal fiber is used, and this part of noise will not be taken into account.

2.1.3.3 Receiver Noise

Optical receivers convert incident optical power P into electric current through a photodiode. The ideal relation between current and optic power is $I = \rho P$, where ρ is the responsivity of the photodiode. However, even for a perfect receiver, there will be noise. Shot noise and thermal noise are two fundamental noise mechanisms which lead to fluctuations in the current even when the incident optical signal has a constant power. The following is to review these two noise mechanisms.

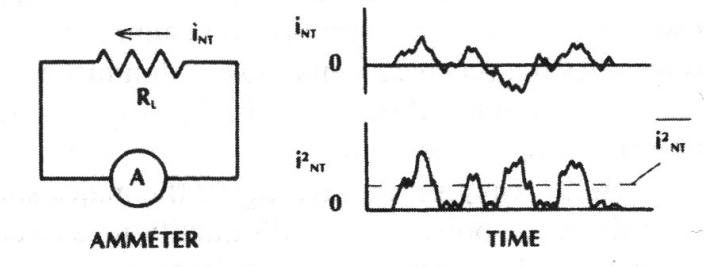

Figure 2.4 Thermal noise current. [22]

Thermal noise comes from the photo-detector's load resistor R_L. Because of thermal energy, electrons within any resistor randomly move, even with no voltage applied. A randomly varying current thus exists in the resistor, as shown in Figure 2.4. This is thermal noise current i_{NT}, and the mean squared value of the thermal noise current $\overline{i_{NT}^2}$ can be calculated as the following,

$$\overline{i_{NT}^2} = \frac{4kT\Delta f}{R_L}$$

where k is the Boltzmann constant, T is the absolute temperature, R_L is the load resistance, and Δf is the electrical bandwidth of the photo-detector. This equation shows that the thermal noise spectrum is uniform over all frequencies and is independent of the optic power. Here only the thermal noise generated in the load resistor is included. An actual receiver contains electrical amplifiers. The amount of noise added depends on the front-end design and the type of amplifiers used. A simple approach accounting for the amplifier noise is as the following [20],

$$\overline{i_{NT}^2} = \frac{4kTF_n\Delta f}{R_{eq}}$$

where F_n is the amplifier noise figure and R_{eq} is the equivalent resistance of photo-detector load and amplifier.

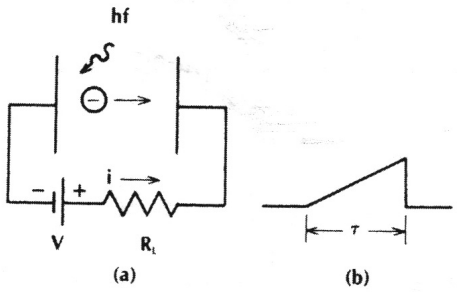

Figure 2.5 (a) Emission of a single photoelectron. (b) Resulting current pulse. [22]

Shot noise is also called quantum noise, and it arises from random generation and recombination of free electrons and holes. In photo-detectors, incoming optic signals generate discrete charge carriers, and each carrier contributes a single pulse to the total current. We illustrate this procedure for the vacuum photodiode in Figure 2.5. When the detector receive an incoming wave having constant optic power P, a large number of pulses as shown in Figure 2.5 will be generated at random time as illustrated in Figure 2.6. The addition of these identical and randomly delayed pulses produces a ragged current which has average value at $I = \rho P$. The deviation from the average current is shot noise.

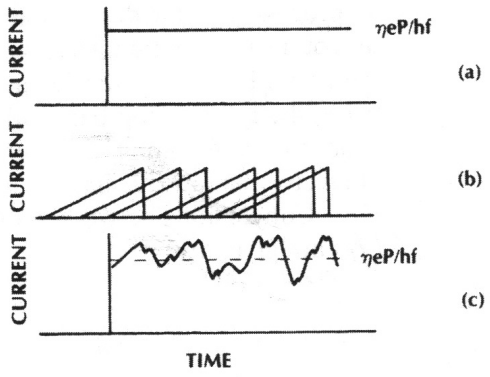

Figure 2.6 Shot noise, (a) Expected (ideal) photocurrent owing to constant optical power P. (b) Randomly produced current pulse created by the emitted electrons, (c) The sum of the current pulses (i.e., the total current). [22]

The mean-square shot-noise current can be calculated by [20]

$$\overline{i_{NS}^2} = 2eI\Delta f = 2e(\rho P + I_D)\Delta f$$

where e is the magnitude of the charge on an electron, I is the average detector current, I_D is the dark current of the photodiode, and Δf is the receiver's bandwidth. One can see that shot noise increases with the rise in the incident optic power.

2.1.3.4 Overall SNR

To analyze the analog system performance, instead of calculating the signal-to-noise ratio (SNR), one usually calculates the carrier-to-noise ratio (CNR). For a sinusoidal signal, the received power at photo-detector can be calculated as [20]

$$P_{carrier} = \frac{1}{2}(m\rho P)^2$$

where m is the optic modulation factor. Then the CNR can be calculated by [20]

$$\frac{C}{N} = \frac{(m^2/2)(M\rho P)^2}{RIN(M\rho P)^2\Delta f + \frac{4kTF_n\Delta f}{R_{eq}} + M^n 2e\Delta f(I_D + \rho P)}$$

Express it in dB-Hz is $$CNR = 10 * \log\left[\frac{(m^2/2)(M\rho P)^2}{RIN(M\rho P)^2 + \frac{4kTF_n}{R_{eq}} + M^n 2e(I_D + \rho P)}\right]$$

where M is the photo-detector internal gain which is unit for PIN photo-detector, and n is an empirically estimated parameter that lies between 2 and 3. We can use some typical values to find how these noises will affect the CNR. Assume we are using a laser with RIN is $-135dB/Hz$, a PIN receiver with $0.8A/W$ responsivity, $2nA$ dark current, and followed by a low noise amplifier with $3dB$ noise figure, and assume the optic modulation factor is 30%. The CNR vs. received optical power is plotted as shown in Figure 2.7. It reveals that at low power level (less than $-15dBm$), the thermal noise dominates; while at high power level, the RIN noise dominates.

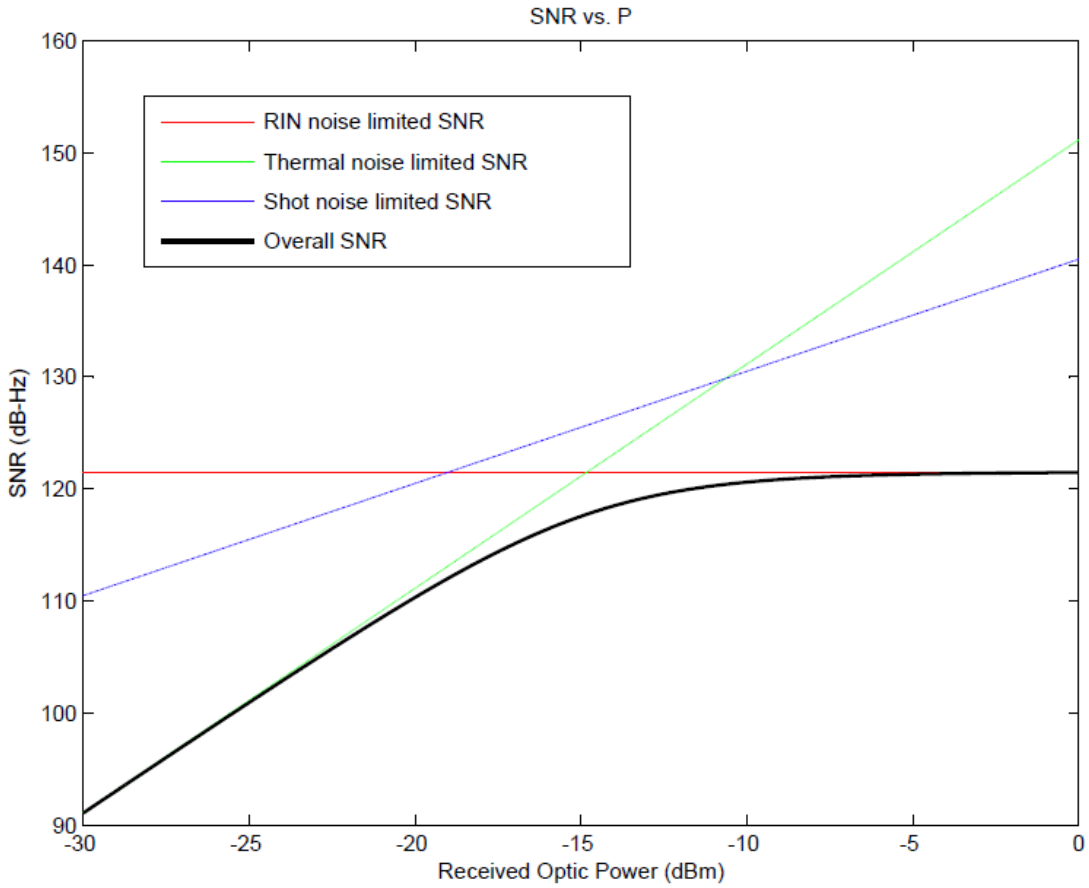

Figure 2.7 CNR vs. detector received optic power for whole bandwidth

From this diagram, based on the SNR required, the photo-detector's sensitivity can be estimated. Let's use a CATV application to approximately estimate the sensitivity of the photo-detector. One CATV channel has 6 MHz bandwidth, and the SNR great than 40 dB, which is 108 dB-Hz, will be considered a good signal quality. From the above diagram, the minimum photo-detector sensitivity should be around -20 dBm.

2.1.4 Linearity

Analog laser/modulator drivers must be highly linear compared with digital transmitters, which means that the transmitted optical power must vary linearly with the input signal voltage. This makes it necessary to use linearization technique. Until now, numerous linearization technologies have been proposed for analog fiber-optic links, such as adaptive pre-distortion method [26], dual-parallel modulation techniques [27], mix polarization techniques [28], feed-forward linearization [29], serially cascaded modulation techniques [30], and analog pre-distortion techniques [31-39]. In the following, we discuss two important linearization techniques: optical feed-forward linearization and pre-distortion linearization.

Figure 2.8 illustrates the principle of Optical feed-forward linearization. A first transmitter (TX1) converts the electrical input signal v_I into an optical signal and introduces distortion. A highly linear receiver (RX) takes part of the transmitted signal using an optical power splitter. The distortion contained is determined by comparing the received signal with the original signal. The inverted distortions then are converted to an optical signal with a second transmitter (TX2) and added to the main signal by an optical power combiner. The output optical signal at the combiner should have no distortion [40].

An average distortion reduction of 20 dB has been achieved with feed-forward linearization applied to a directly modulated transmitter [41].

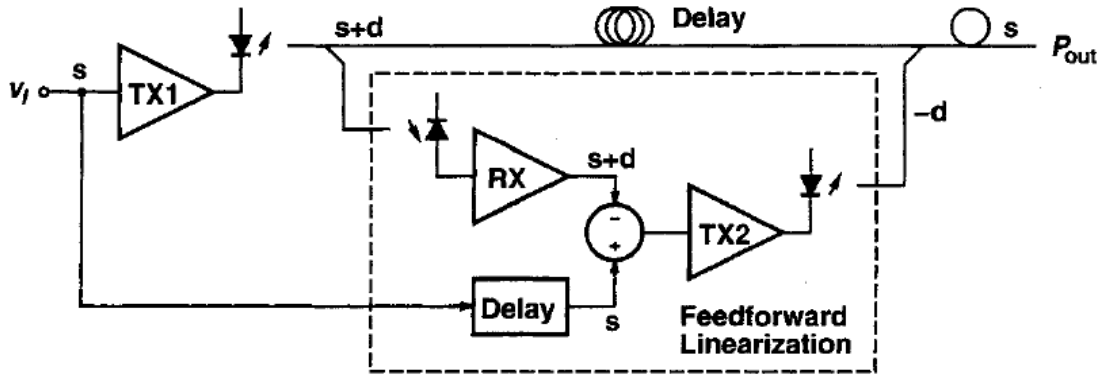

Figure 2.8 Principle of optical feed-fordward linearization [40]

Another important method to reduce distortions is pre-distortion linearization. The analog signal is pre-distorted by the inverse function of the transmitter's nonlinearity before it is fed into the transmitter. Ideally, the pre-distortion nonlinearity and the transmitter nonlinearity cancel each other, and thus the optical output signal should be linear to the original input signal.

The use of a linearization technique can significantly improve the linearity of the system, and the pre-distortion method will be used for our system. The detail will be shown in another thesis and will not be discussed here.

2.1.5 Selection of Light Source and Photo-Detector

This section will provide the selection of light source and photo-detector based on the analysis above and other considerations.

2.1.5.1 Light Source

LD and LED are the two most common light sources in communication system because of their inherent advantages such as compact size, high efficiency, good reliability, right wavelength range, and small emissive area compatible with fiber core dimensions [42].

The LED operates on spontaneous emission. A LED is simply a forward biased p–n homo-junction. Light generated by radioactive recombination of electron–hole pairs in the depletion region. The emitted light is incoherent with a relatively wide spectral width and a relatively large angular spread. Figure 2.9 and Figure 2.10 illustrate the power-current relationship of a LED. Because there is no mechanism to select a single wavelength, the spectral line-width is very wide, typically $\Delta\lambda_S = 50 \sim 60nm$. Moreover, the carrier lifetime τ limits the 3-dB modulation bandwidth, $f_{3-dB} = \frac{1}{2\pi\tau}$, to a few hundred MHz [42]. So their application is mostly in short-reach data communication systems using Multi Modal Fiber (MMF) and cannot be used in our system.

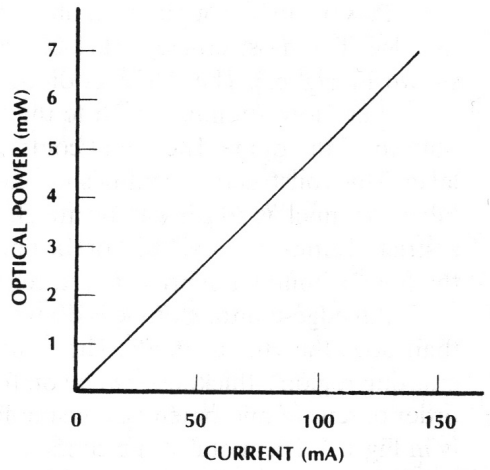

Figure 2.9 Power-current relationship for a LED. [42]

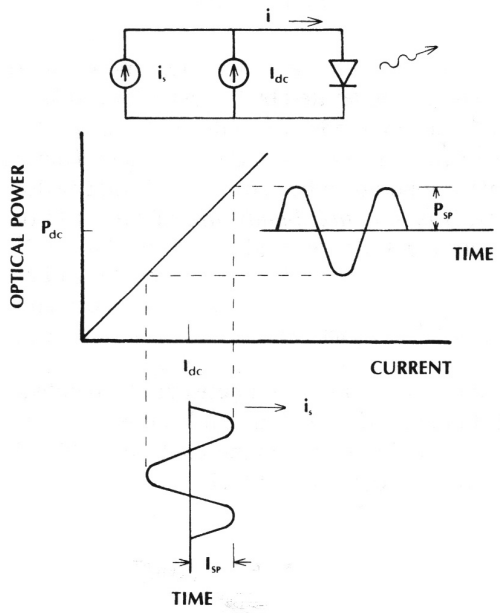

Figure 2.10 Analog modulation of a LED. I_{dc} is the dc bias current, and i_s is the signal current. [42]

Semiconductor laser emits light by stimulated emission, and thus it has narrow spectral width of emitted light $\Delta\lambda_S = 1 \sim 5nm$, and can be modulated directly at high frequencies because of a short recombination time associated with stimulated emission. Its power-current relationship is shown in Figure 2.11 and Figure 2.12. Laser will be chosen for our system.

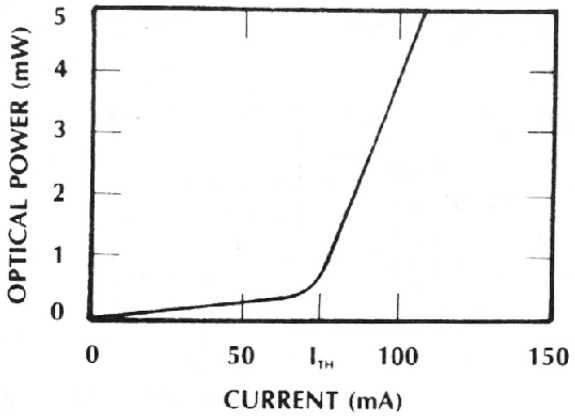

Figure 2.11 Power-current relationship of a LASER. [12]

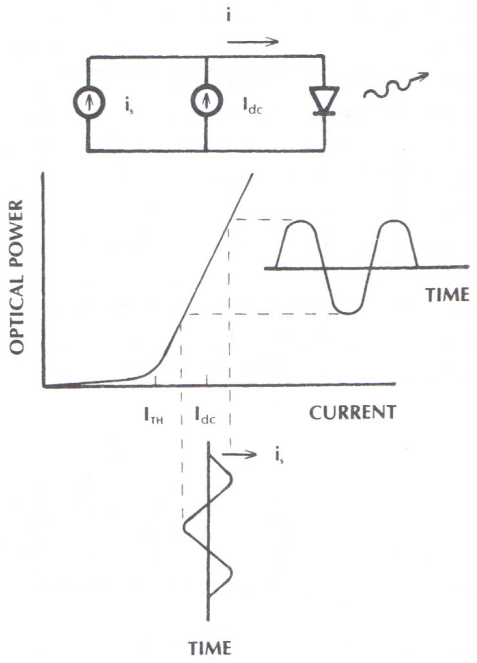

Figure 2.12 Analog modulation of a laser diode [12]

Among many type of lasers, the Fabry-Perot (FP) laser, the distributed-feedback (DFB) laser, and Vertical-Cavity Surface-Emitting Laser (VCSEL) are the most commonly used lasers in telecommunication systems.

The FP laser consists of an optical gain medium located in a cavity formed by two reflecting facets, as shown in left-hand side of Figure 2.13(a). The wavelengths at which the laser can operate are determined by the separation of the two facets and the cavity length. FP lasers belong to the class of multiple-longitudinal mode (MLM) laser, and the spectrum of the emitted laser light has multiple peaks, as shown on the right-hand side of Figure 2.13(a). The spectral line-width is typically around 3 nm. FP lasers are mostly used at the 1.3 um wavelength where dispersion in an SMF is low. Most FP lasers are operated as un-cooled lasers, their temperature is not controlled. This can simplify the transmitter design and keeps its cost low. [44]

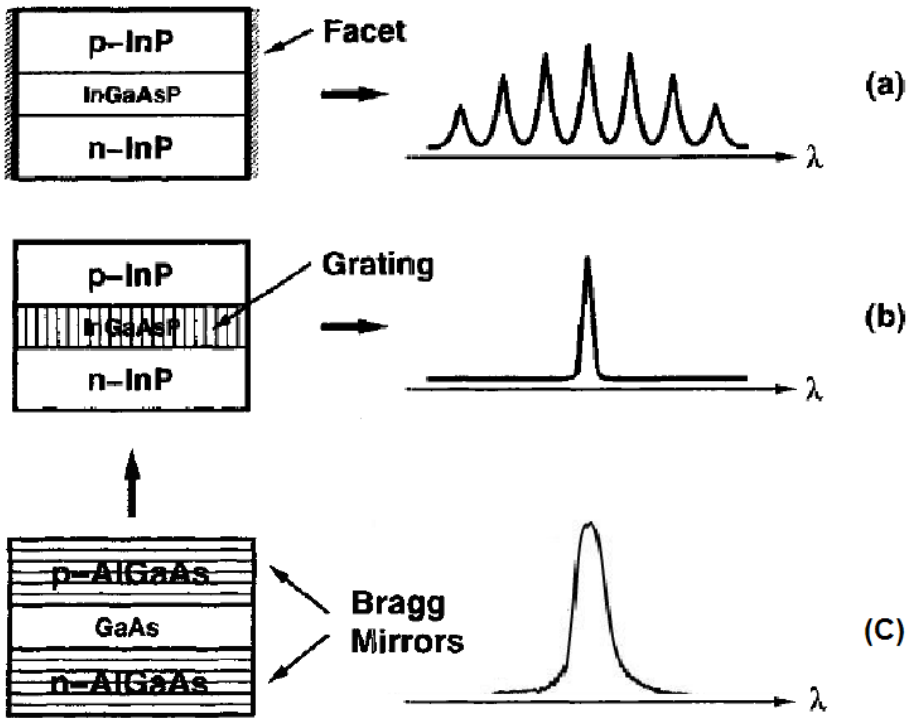

Figure 2.13 (a) Fabry-Perot laser. (b) distributed-feedback laser. (c) vertical-cavity surface-emitting laser. The light propagates in the direction of the arrow. [44]

The DFB laser consists of a similar gain medium as in an FP laser, with a built-in grating as shown in Figure 2.13(b). The grating provides distributed feedback and selects only one wavelength for amplification as shown on the right-hand side of Figure 2.13(b). So, DFB lasers belong to the class of single-longitudinal mode (SLM) lasers. The emitted spectrum of a modulated DFB laser has a very narrow line-width, typically less than 1nm. DFB lasers are suitable for direct modulation as well as for CW sources followed by an external modulator. The temperature change can cause the variation in the wavelength emitted by a semiconductor laser, typical 0.1 nm/^{o}C a DFB laser. For this reason, the laser temperature must be controlled precisely. DFB lasers are operated as cooled lasers., as a result, such lasers are mounted on top of a thermoelectric cooler (TEC) to stabilize the temperature. [44]

The FP or DFB lasers emit light at the edges of the chip, whereas the VCSEL emits the light perpendicular to the wafer surface. The VCSEL consists of a gain medium located in a very short vertical cavity as shown in Figure 2.13(c). Because of the short cavity length, the VCSEL also belongs to the class of SLM laser. However, VCSELs have multiple transverse modes depending on the horizontal size, resulting in a wider spectral line-width than the DFB lasers. The very short length of the gain medium requires mirrors with a very high reflectivity. Currently, VCSELs are available at short wavelengths ($0.85\mu m$ band) and Long-wavelength VCSELs are under development. [44]

The wavelength of our system is 1310 nm, so VCSEL is not a suitable option. Because the line-width is not critical at this wavelength, the FP laser will be chosen by virtue of its lower cost and easier operation (un-cooled) compared to the DFB laser.

In the current market, the 1310 nm FP laser has several kinds of packages: laser diode chip, transistor outline-can (TO-Can), Transmit Optical Sub-Assembly (TOSA), and butterfly. Figure 2.14, Figure 2.15, and Figure 2.16 show some products of those packages. The laser diode chip and the TO-Can laser are very cheap. However, their input impedance is not matched and they need additional fiber connection, which will complicate our design and thus are not appropriate choices for our system. In contrast, the butterfly package includes everything in a single package and can stand alone as an independent transmitter, but it has higher cost and bigger volume. The TOSA package is in the between enabling the simplification of design at low cost and compressed size, so the TOSA will be chosen for our system.

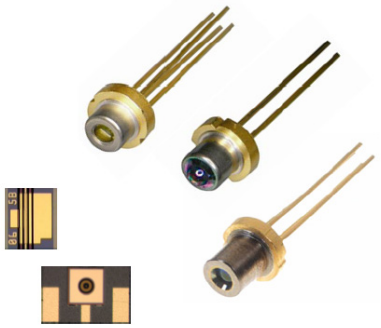

Figure 2.14 1310 nm laser chips and TO-can products

Figure 2.15 1310 nm TOSA products

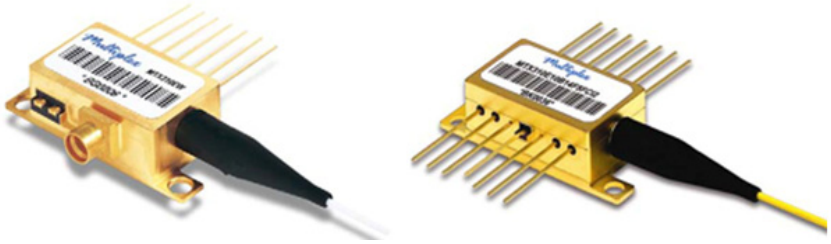

Figure 2.16 1310 nm butterfly packaged lasers

2.1.5.2 Photo-detector

In telecommunication system, there are two kind of photo-detectors that are widely used, namely p-i-n photo-detector (PIN) and avalanche photo-detector (APD).

The simplest detector is PIN, as shown in Figure 2.17. A PIN is simply a p-n junction with an intrinsic semiconductor layer sandwiched in between. The junction is reverse biased to create an electric field in the intrinsic material. Photons incident on the intrinsic layer create electron-hole pairs, which separated by the electric drift field. Thus, a photocurrent appears at the terminals with the relationship $I_{PD} = \rho P$, where ρ is the photo-detector responsivity and P is the incident power.

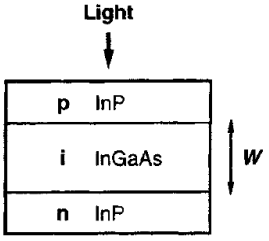

Figure 2.17 p-i-n photo-detector (schematically) [45]

The basic structure of the APD is shown in Fig. 3.5. The avalanche photo-detector is also a reverse biased diode like the PIN detector. However, in contrast to the PIN photo-detector, it has an additional layer, the multiplication region. This layer provides gain

through avalanche multiplication of the electron-hole pairs generated in the intrinsic layer. The photocurrent is $I_{PD} = M\rho P$, where M is the current gain. The APD has to be operated at a higher reverse bias than PIN, about 40 to 60 V. [45]

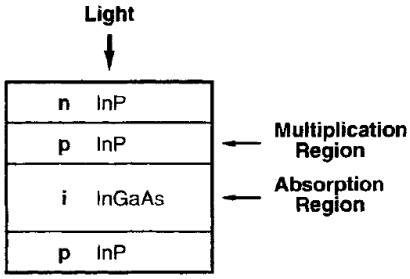

Figure 2.18 Avalanche photodetector (schematically). [45]

The current gain for the APC photo-detector leads to higher sensitivity and higher SNR than PIN. However, the APC will work under much higher DC source, and it entails higher cost. Since the noise analysis reveals that the PIN photo-detector can satisfy our system requirements, we will choose PIN photo-detector. PIN photo-detector has the same package as laser diode, PD chip, TO-Can, receive optical sub-assembly (ROSA), and butterfly. Due to the same rationale for the light source, we will choose the ROSA package for our design.

2.2 Monitor and Control

In order to ensure the proper functioning of the transceiver, one needs to control it and monitor its performance during operation. The main control function is the LD driver control.

Figure 2.11 in previous section illustrates the power-current relationship of a laser. This is actually the relationship at specified temperature. Laser diode is very temperature sensitive, and Figure 2.19 illustrates the temperature dependence of a representative laser diode. It clearly shows that the laser diode threshold current increases when the temperature rises, and thus the output optic power decreases if the current has no change. The junction temperature will change while laser is working and the environment temperature is not constant also, so standard laboratory power supply is not suitable for driving a laser diode. There are two techniques commonly used to achieve a stable optical output from a laser diode: thermoelectrically cooling the diode while keeping the bias current constant, and varying the bias current to keep the output optic power constant.

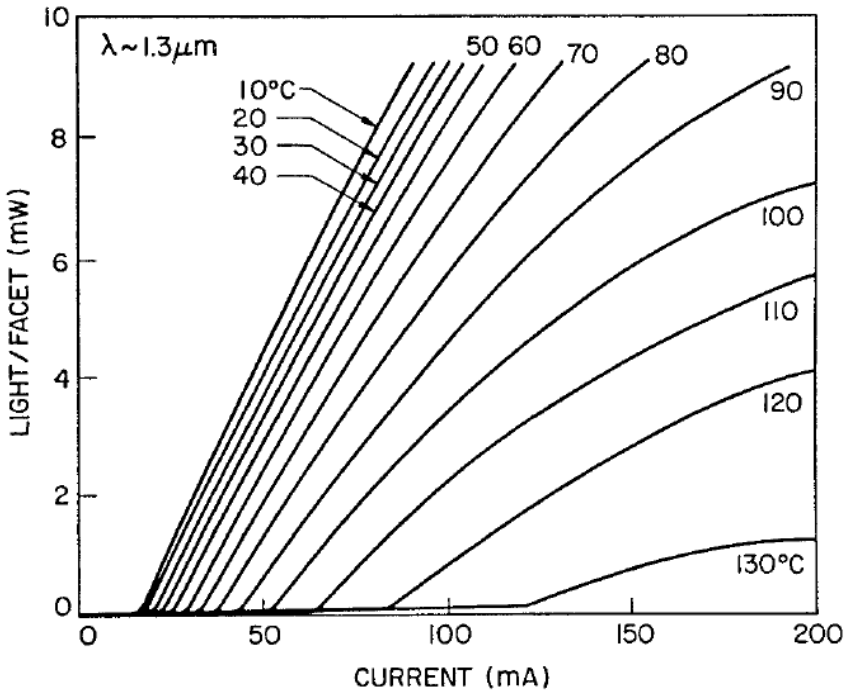

Figure 2.19 Temperature dependence of a LASER diode [24]

A thermoelectric cooler is a semiconductor junction device whose temperature depends on the direction of the current flow. The laser diode is mounted on the cooler. The diode's temperature is stabilized via changing the current through the thermoelectric cooler base on the temperature detected by a thermistor heat detector. Then the laser is operated by a constant current. The advantage of this technique is narrow spectral width of emitted light, good linearity, and longer life time. It is not used in our system, however, due to its drawbacks in complicating the control circuit and increasing the cost accordingly.

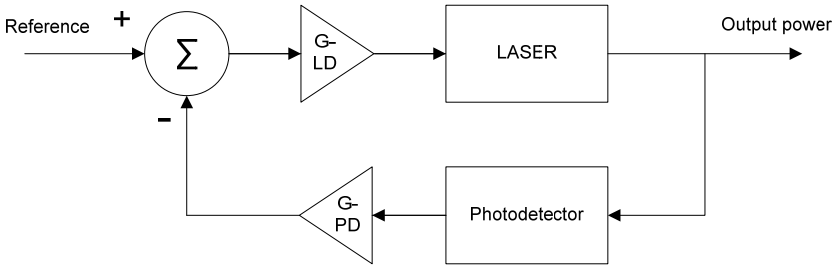

Figure 2.20 APC block diagram

In the constant output power technique, the output power will be constant at different temperature by varying the bias current. From Figure 2.19, one can see that for temperature from 10° to 80°, at lower power level, the slop of power-current curve is very close, which means if we keep the output power constant, the signal degradation due to temperature change is not critical. An automatic power control (APC) circuit is needed to keep the power constant. Its principle is a simple feedback loop as shown in Figure 2.20. The actual change of the laser output is measured by a photo-detector. The DC current is then changed accordingly to bring the optic power back to the desired value. A simple APC circuit is provided as shown in Figure 2.21. A photodiode generates a current

which is proportional to the transmitted optical power. This current passes the R and C low-pass filter, thus the node x voltage will be proportional to the average optical power. An operational amplifier compares the node x voltage with the reference voltage V_{REF} to generate the control voltage to control the laser's bias current I_B, so that the desired average optical power set by V_{REF} is obtained. This technique will be chosen for our design.

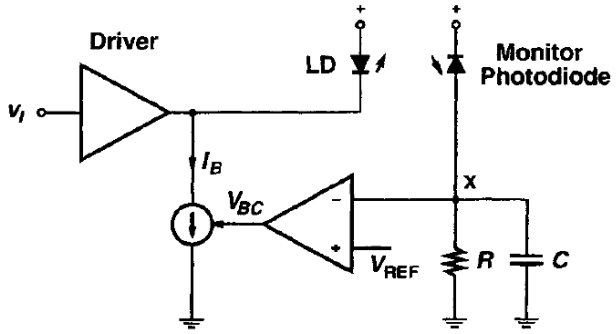

Figure 2.21 APC circuit [25]

To make sure the proper and safe operation of the system, one needs to monitor many information such as whether the source voltage is out of the desired range, whether the environment temperature is too high or too low, whether the bias current is close to the maximum value, whether the received optic power is too high to destroy the PD or too low to get qualified signal, and so on. Moreover, for the purpose of automatic operation, alerts should also be provided for abnormal operation conditions.

In modern electronics, a microcontroller can be used to complete monitor and control functions. Due to the optical application is widely used, and many companies provide special controllers which are used for optical transceivers only. With compatible price as

that of general microcontroller, this controller integrates almost all the functions needed for the optical transceiver. For this reason, we will select such a chip for our system.

CHAPTER 3 SYSTEM SIMULATION

Based on the analysis in the previous section, we use the OptiSystem to simulate our design so as to verify the photo-detector sensitivity that we need. Assume we need to use this transceiver for a RoF application which needs to transmit 10-channel CATV signals starts from 471.25 MHz at 6 MHz spacing and one 1.7 GHz amplitude modulation (AM) carrier modulated by 1Gbit/s digital signal. We use those typical values which used to analyze the system in the last chapter and to construct the OptiSystem circuit as shown in Figure 3.1.

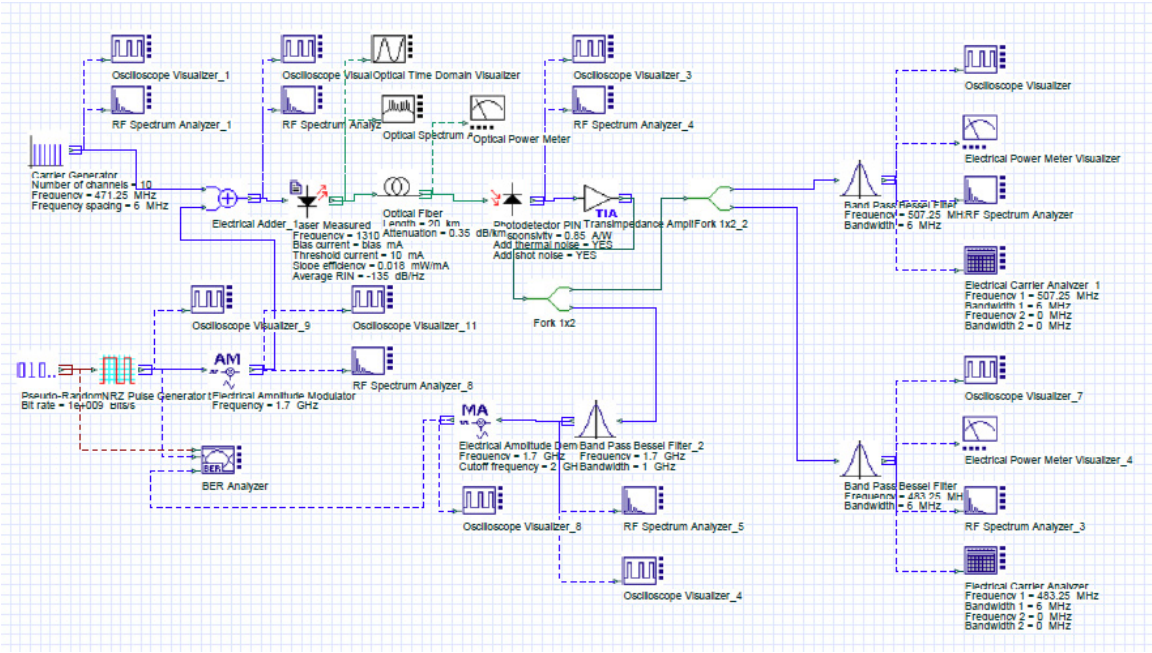

Figure 3.1 Simulation circuit

A carrier generator generates 10 sinusoidal waves starting at 471.25 MHz at 6 MHz spacing, and a bits generator generates a 1 Gbit/s digital signal to modulation a 1.7 GHz

carrier by the AM modulator. These signals combine and then directly modulate a 1310 laser with -135dB/Hz RIN noise. The output optic power is transmitted by 20 km single modal fiber with 0.35dB/km attenuation and reaches a PIN photo-detector with 0.80A/W responsivity. The signal output by the photo-detector is then filtered at each frequency band to recover the original signal. We can measure the SNR for the analog signal and the BER for the digital signal to qualify them.

By way of adjusting the laser output power, which is indeed by way of changing the photo-detector received power, the SNR and the BER versus the photo-detector received optic power is plotted in Figure 3.2. From the diagram, we can find that to achieve SNR great than 40 dB and good BER ($<10^{-12}$), the received power should be great than -16 dBm, which is 4 dBm higher than our calculation result. Figure 3.3 and Figure 3.4 show the signal flow in time domain and in frequency domain at -12 dBm received optic power, and Figure 3.5 shows the eye diagram as well as the SNR.

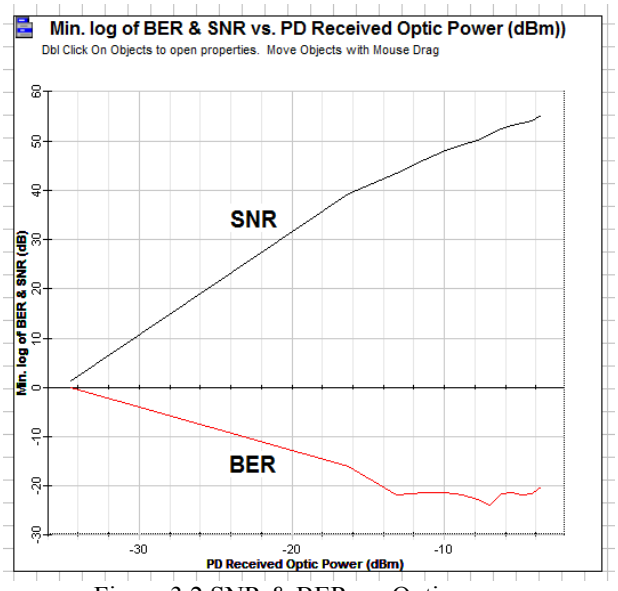

Figure 3.2 SNR & BER vs. Optic power

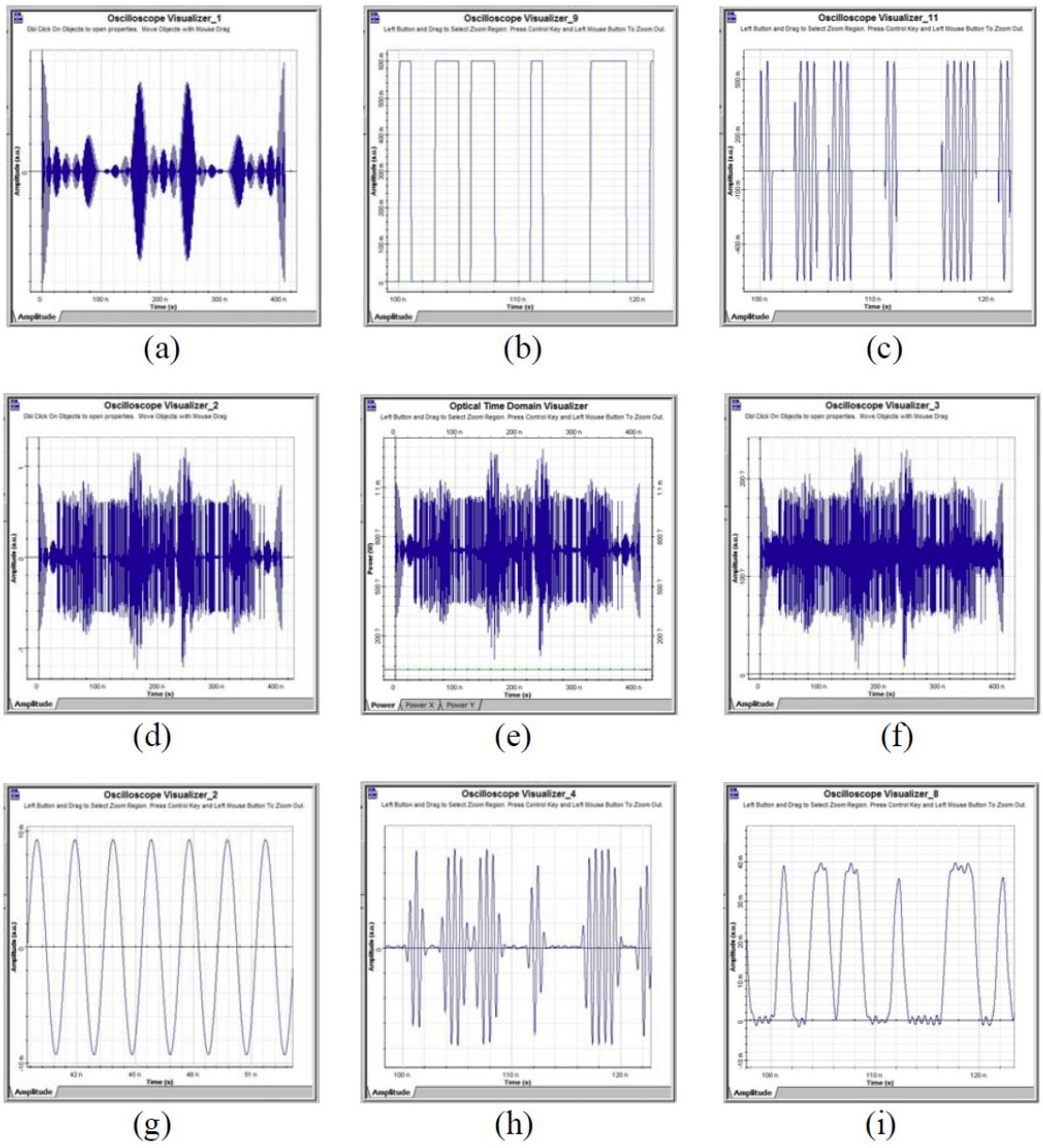

Figure 3.3 Signals in time domain. (a) generated 10 channels CATV signals, (b) generated digital signal bits sequence, (c) bits sequence AM signal, (d) combined a and c, (e) optic signal generated by laser, (f)generated signal by PD, (g) recovered CATV signal at 507.25 MHz, (h) received AM signal after filter, (i) recovered digital bits sequence.

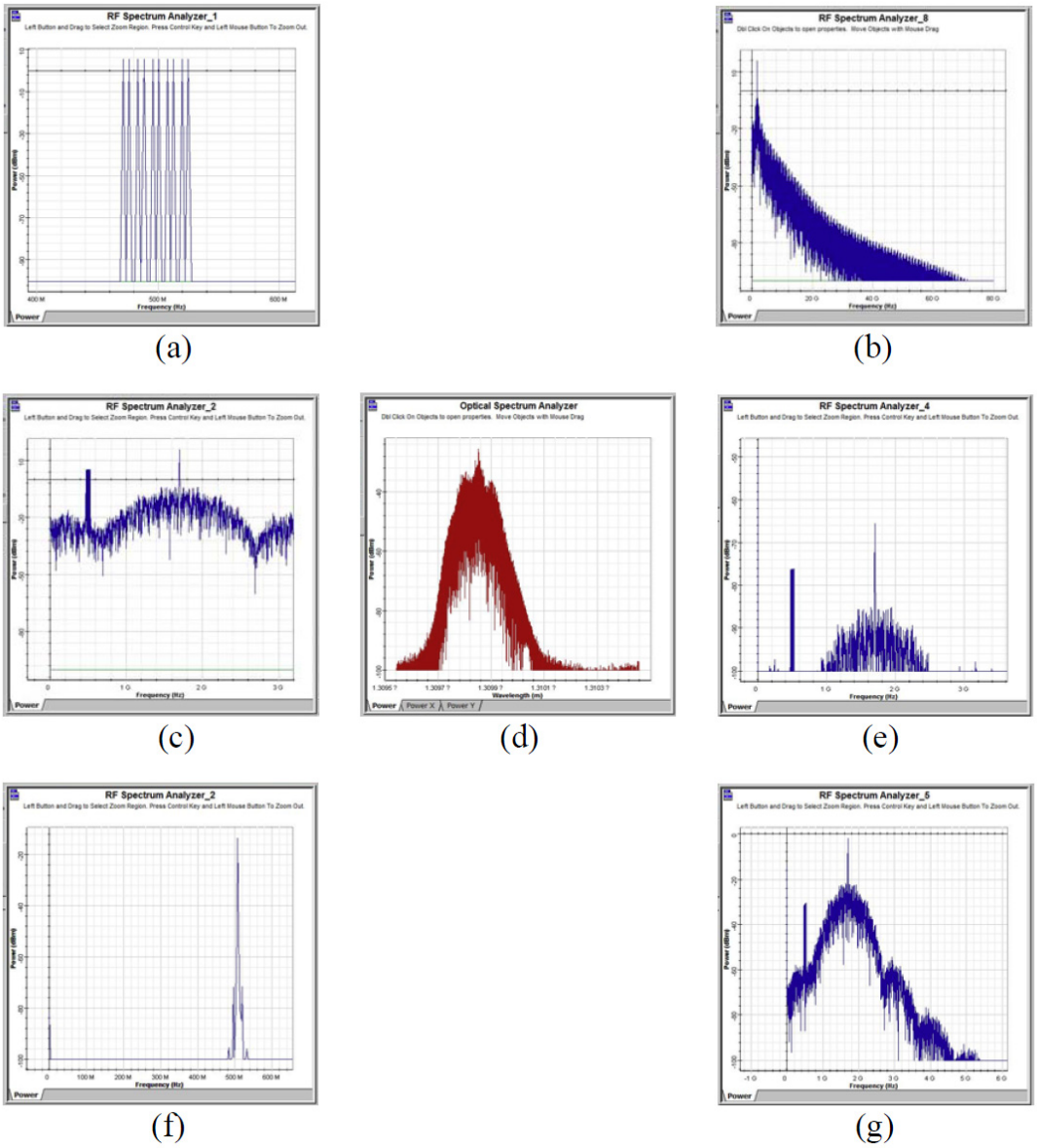

Figure 3.4 Signals in frequency domain, (a) generated 10 channels CATV signals, (b) generated AM signal, (c) combined signal of a and b, (d) optic signal generated by laser, (e) generated signal by PD , (f) recovered CATV signal at 507.25 MHz, (g) received AM signal after filter.

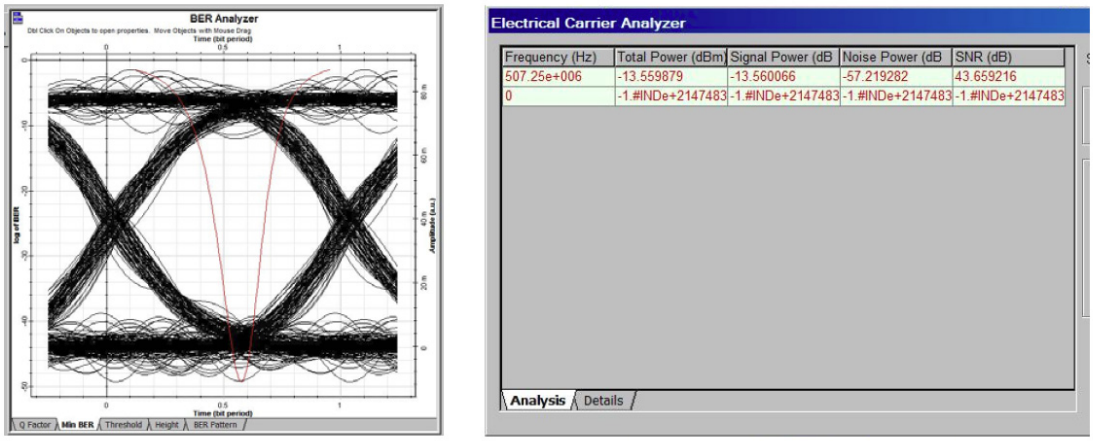

(a) (b)

Figure 3.5 (a) eye diagram of recovered digital signal, (b) SNR of recovered CATV signal at 507.25 MHz

CHAPTER 4 PRODUCT FABRICATION

Based on the analysis and simulation accomplished in the previous two chapters, we summarize the requirements for each component and present selection and product fabrication in this chapter.

4.1 Light Source

The requirements of the light source is summarized as following,

- Source type: FP laser
- Wavelength: 1310 nm
- Package: TOSA
- Output power at operation point: 0 dBm (1 mW)
- Rise time: $t_{rise} < 37 ps$
- RIN noise: around -135 dB/Hz
- Feedback photo-detector integrated
- Impedance is matched inside the package

A research in the current market reveals that the laser FP-1310-10LRM-LCA produced by Finisar Inc. is the best option for our design. The laser pin out and some of its parameters are shown in Figure 4.1 and Table 4-1, respectively.

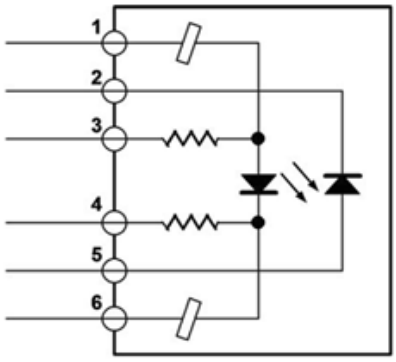

PIN	Function
1	Bias +
2	MPD-C
3	Mod +
4	Mod -
5	MPD-A
6	Bias -

Figure 4.1 FP-1310-10LRM-LCA TOSA

Table 4-1 Parameters of FP-1310-10LRM-LCA

	Value	Unit
Forward voltage	1 ~ 1.6	V
Threshold current	10 - 25	mA
Operating current	45	mA
Output power	-1.5	dBm
Slope efficiency	0.018	mW/mA
Monitor current	200 ~ 2000	uA
Wavelength	1295 - 1315	nm
Spectral width	1.4	nm
Relative intensity noise	-136	dB/Hz
Rise/Fall time	35	ps
Operation temperature	-5 ~ 85	ºC
Maximum forward current	130	mA
Input impedance	50	ohm
Optical interface	LC receptacle	

4.2 Photo-Detector

The requirements of photo-detector is listed as following,

- Photo-detector type: PIN photo-detector
- Package: ROSA
- Wavelength: 1310 nm
- Responsicity great than 0.8 A/W
- Maximum input optic power: 3 dBm (2 mW) peak or more
- Rise time: $t_{rise} < 37 ps$
- Trans-impedance amplifier integrated
- Impedance is matched inside the package

The photo-detector PIN-1310-10LR-LC produced by Finisar Inc. is good for our design. The pin out and some parameters of the photo-detector are shown in Figure 4.2 and Table 4-2, respectively.

PINOUT:

PIN	Description
1	Vcc
2	CASE
3	OUTP
4	OUTN
5	CASE
6	V_{PD}

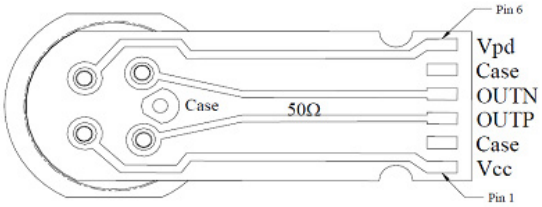

Figure 4.2 PIN-1310-10LR-LC ROSA

Table 4-2 Parameters of PIN-1310-10LR-LC

	Value	Unit
Supply voltage	3.0 ~ 3.6	V
Input optic wavelength	1260 ~ 1620	nm
PD responsivity (1310 nm)	0.85	A/W

Total responsivity	1500	V/W
PD bias	3.0 ~ 3.6	V
Output impedance	50	ohm
Rise/Fall time	35	ps
Operation temperature	-10 ~ 85	ºC
Maximum incident average optic power	3	dBm
Maximum incident average peak power	5	dBm
Optical interface	LC receptacle	

4.3 Controller

MIC3003GML produced by Micrel Inc. as shown in Figure 4.3 is chosen as the controller for our system. MIC3003 is a fiber optic controller for fiber optic transceivers with intelligent laser control and an internally calibrated Digital Diagnostic Monitoring Interface. It has advantages as listed subsequently,

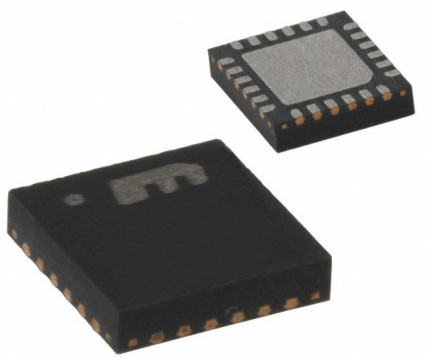

Figure 4.3 MIC3003GML laser diode controller

- Highly configurable automatic power control (APC) circuit

- Integrated digital temperature sensor

- An analog-to-digital converter converts the measured temperature, voltage, bias current, transmit power, and received power from analog to digital, and each parameter is compared against user-programmed warning and alarm thresholds

- An analog comparator and DACs provide fast monitoring of received power and critical laser operating parameters

- Monitors report critical parameters: temperature, bias current, TX and RX optical power, and supply voltage

- A power-on hour meter logs operating hours using an internal real-time clock and stores the result in NVRAM

- 3.0V to 3.6V power supply range

- Small size: $4mm \times 4mm$

- Software provided to communicate with the controller chip via computer

4.4 Interfaces

Based on the above mentioned components selection, there will be below interface for the transceiver.

RF interface: the frequency range of the system is 6 GHz, and a general SMA connector can handle this frequency. The 142-0701-801 SMA connector (shown in Figure 4.4) produced by Johnson Components Inc. is chosen for our design.

Optical interface: both the TOSA and ROSA have LC receptacle, so the LC connector as shown in Figure 4.5 is choose for our design.

Monitor and control interface: the chip company provides software which can run in a computer to monitor and control the chip via a USB interface, so the transceiver control interface is a USB connector as shown in Figure 4.6.

Power interface: a simple 5 V DC source is sufficient for the transceiver, so a two wires cable is used for our power line.

Figure 4.4 142-0701-801 SMA connector

Figure 4.5 LC optical connector

Figure 4.6 USB connector (A type for one side and B type for the other)

4.5 Substrate and Transmission Line

The transceiver will be fabricated on printed circuit board (PCB). The PCB board needs to handle 6 GHz frequency and be strong enough to support all components and the operation of the transceiver. Its transmission line width should be compatible with the TOSA and ROSA signal pins and the SMA connector signal pin. On one hand, the board needs to be sufficiently thick to ensure an adequate strength. On the other hand, the transmission line width needs the board to be thin to a certain extent. We choose Rogers Inc. RO4003C 32mil as our substrate. With the use of the Advanced Design System (ADS) line calculator, the transmission line width is calculated (55.5 mil) as shown in Figure 4.7. A simple transmission line was fabricated before the overall fabrication in order to test its performance. The S-parameters of this transmission line measured by a network analyzer is shown in Figure 4.8. Both S11 and S22 are below -20 dB which means the transmission line is very good matched.

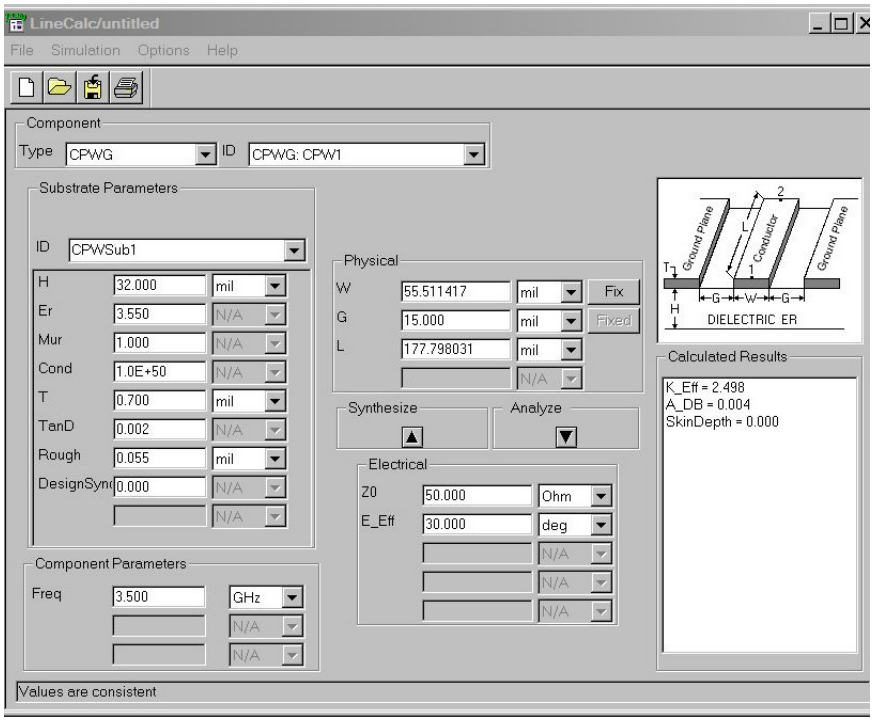

Figure 4.7 Transmission line width calculation by ADS line calculator

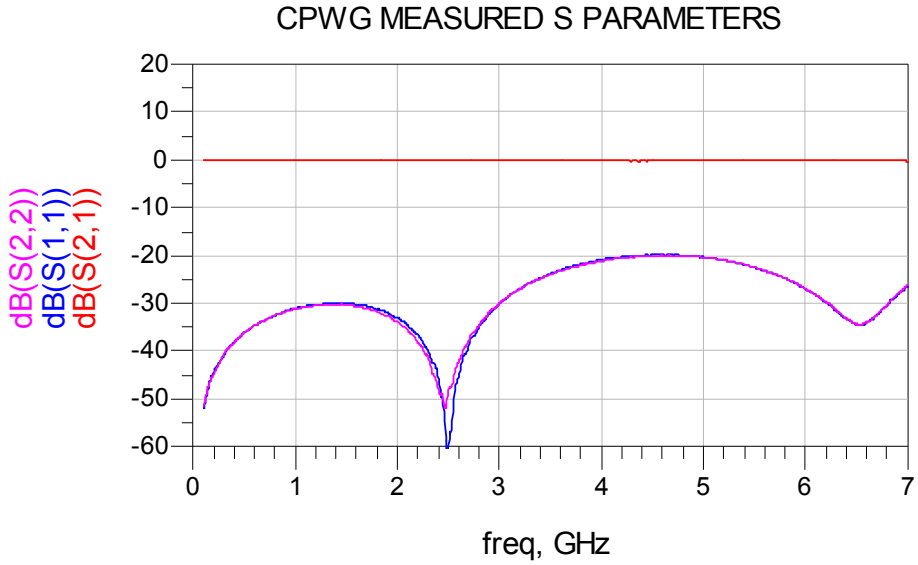

Figure 4.8 S Measured S parameters of transmission line

4.6 Overall Circuit

To facilitate the test and the debugging of the system, the transceiver is separated into two circuits, AC and DC. The DC part performs the control function and the AC part performs the signal transmission. The overall circuit diagram and components list are attached in Appendix B. The fabricated two circuits are shown in Figure 4.9. Figure 4.10 shows the connection of the two circuits and the overall system interfaces.

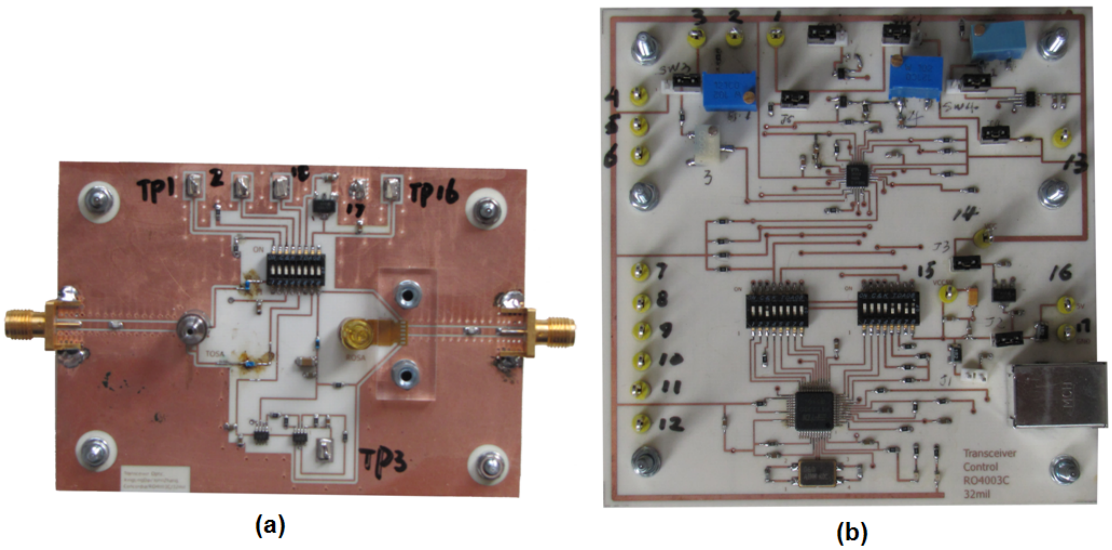

(a) (b)

Figure 4.9 Fabricated transceiver (a) AC circuit, (b) DC circuit

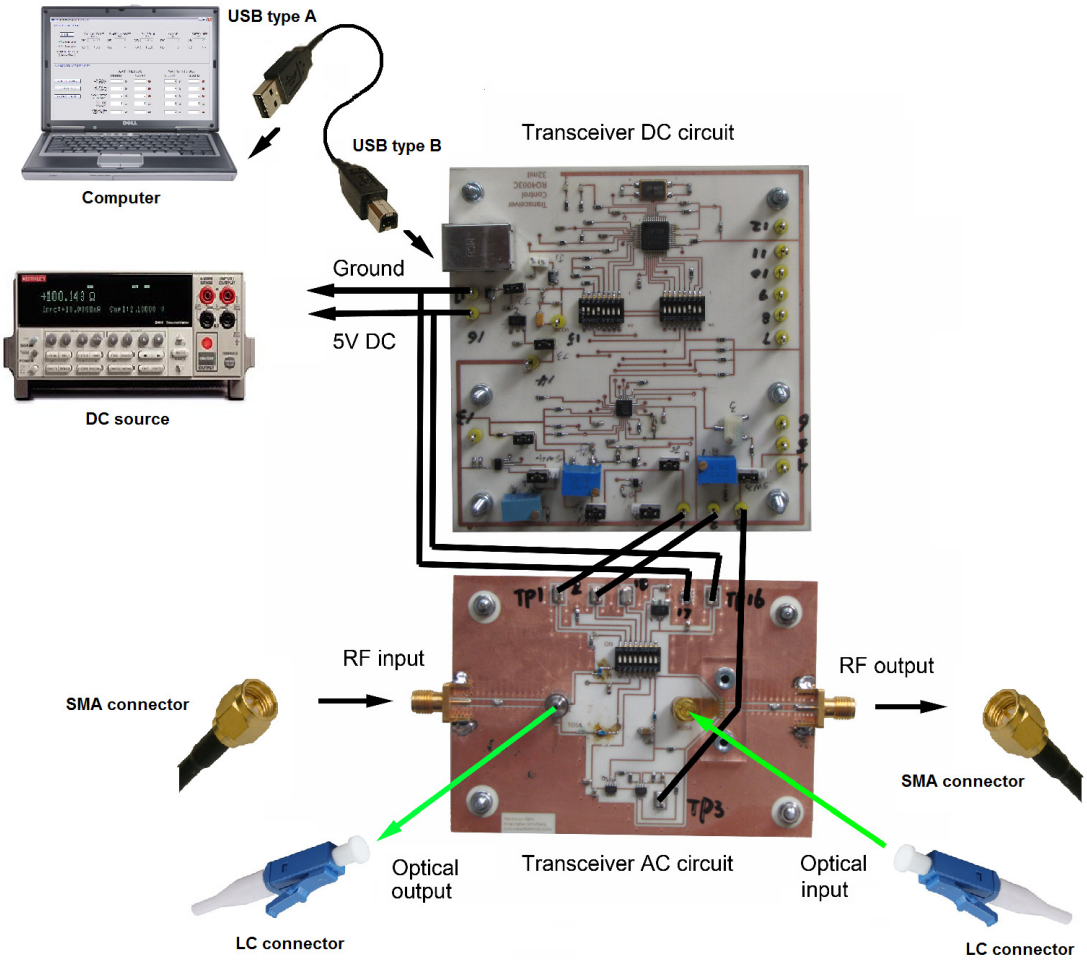

Figure 4.10 Overall transceiver connection and interfaces

4.7 Link Performance Estimation

Optical links performance can be measured as the same way used to characterize RF components. To do so, one will assume a short single-mode fiber links the laser and photo-detector. So the dispersion and nonlinearity in the fiber can be ignored and we just consider the intrinsic link [43]. Based on the given parameters of laser and photo-detector, we can estimate some important link parameters as the following.

- Link gain

The laser has slop efficiency of 0.018 A/W, and the photo-detector has total responsivity of 1500 V/A. Input signal current i will result in output signal voltage $0.018 \times 1500/2 \times i$, and thus the power gain is $\frac{P_{out}}{P_{in}} = \frac{(0.018 \times 1500/2 \times i)^2 / R_S}{i^2 \times R_S} = 0.0729 = -11dB$, where R_S is 50Ω.

- Link bandwidth

$$f_{3-dB} = \frac{0.35}{t_S} = \frac{0.35}{\sqrt{t_{LS}^2 + t_{PD}^2}}$$

The rise time of laser and photo-detector are both $35ps$, this results $f_{3-dB} \approx 7GHz$

- Link noise figure

An approximate formula to calculate the noise figure is given by [43],

$$NF = 10\log(1 + CONSTANT + \frac{1}{g_i} + \frac{I_D^2 RINR_S}{kTg_i} + \frac{2qI_D R_S}{kTg_i})$$

where $CONSTANT$ expresses the effect of the unavoidable source of added thermal noise arising in the modulation device circuit and is set to 2 here, g_i is the intrinsic link gain, I_D is the average photo-detect current which is the laser output power times the photo-detect responsivity, RIN is the laser relative intensity noise, R_S is the RF source resistance which is 50Ω, k is the Boltzmann constant, T is the absolute temperature, and q is the magnitude of the charge on an electron. Based on the parameters given, and

assume the laser output $1mW$ optic power at room temperature, the noise figure can be calculated as $NF \approx 31dB$.

CHAPTER 5 EXPERIMENTAL VERIFICATION

The transceiver is well fabricated. Several experiments will be done to demonstrate that this product can work as we expected. The following section will show the experiments detail and result.

5.1 Transmitter Evaluation

The role of the transmitter is receiving electric signal and converting it to optic signal and then launching it into the fiber. The transmitter should be input impedance matched to ensure maximum signal power flow into the laser; it should have enough output optic power to transmit the signal to the receiver; within the desired bandwidth, the variation of the gain should be less than 3 dB. The transmitter part of our transceiver was evaluated in both DC and AC performance. The DC evaluation circuit was constructed as in Figure 5.1. The optical output was connected to an optical power meter via a one meter single modal fiber. By varying the source current I_source from 0 to 120 mA, we read the optic power meter to get output optic power and read the voltage meter to get the PD feedback current. The transmitter DC performance was plotted in Figure 5.2 and Figure 5.3.

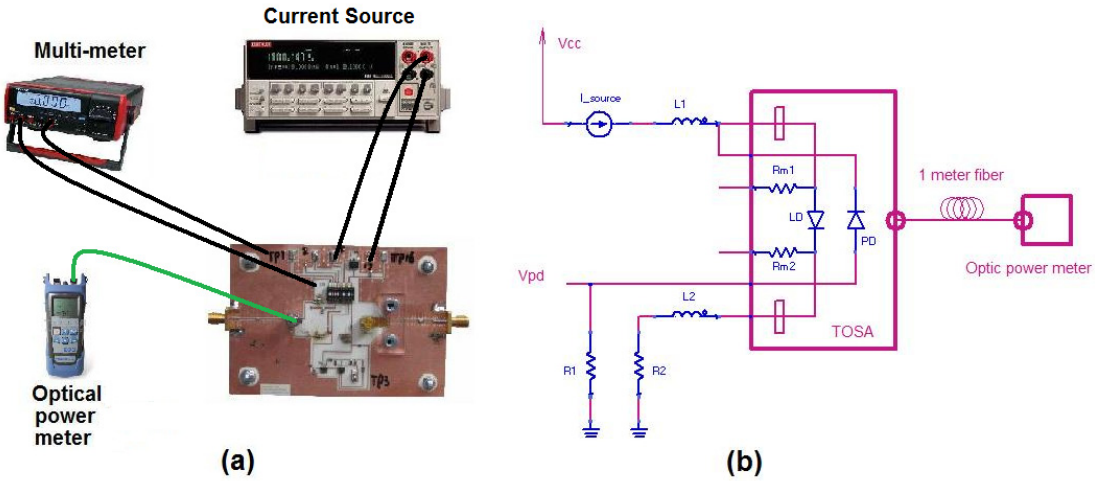

Figure 5.1 Transmitter DC evaluation circuit (a) components connection, (b) circuit schematic

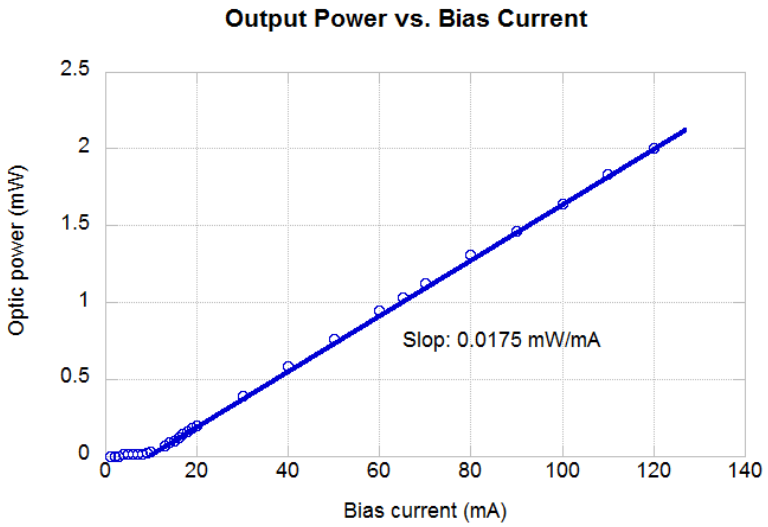

Figure 5.2 Measured TOSA P-I characteristic

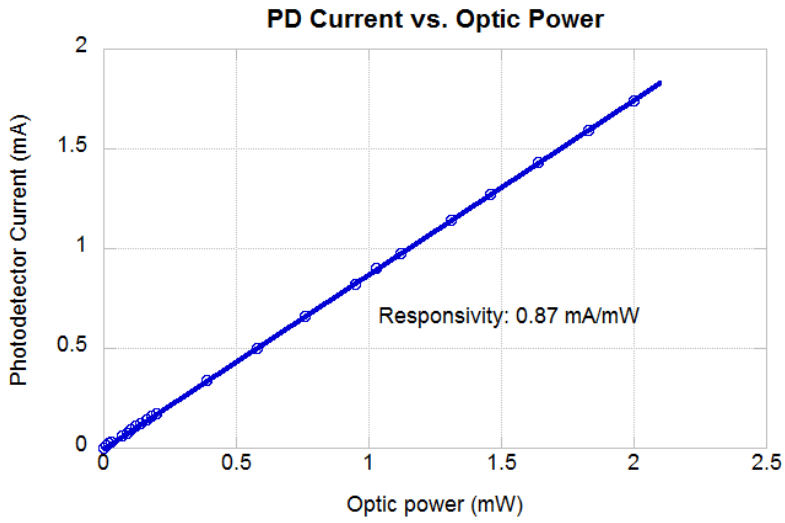

Figure 5.3 Measured TOSA PD I-P characteristic

The results show both the output power and PD feedback current have very good linearity within this current range. The power budget calculation result needs the output power to be greater than 0 dBm (1 mW). The measurement above is actually the power measured after coupling loss, so the minimum required power should be $0dBm - 3dB = -3dBm$ (0.5 mW). From the result figure, we can see that the transmitter has enough output power just by setting the bias current at great than 40 mA.

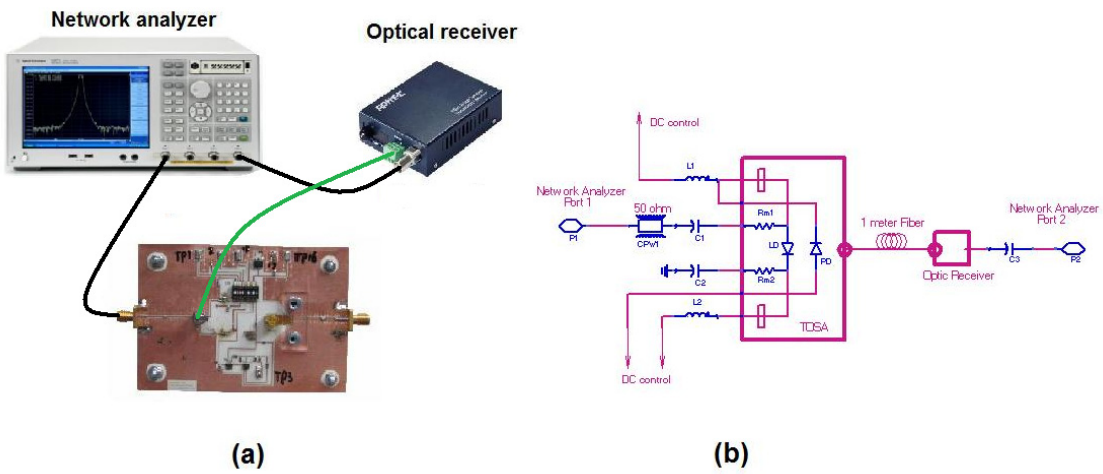

Figure 5.4 Transmitter AC evaluation circuit (a) components connection, (b) circuit schematic

The AC evaluation circuit was constructed as shown in Figure 5.4. The bias current is set to 50 mA (for simplicity, the DC connection is not presented in the figure) and the transmitter output optical signal is directly detected by a high-speed optic receiver with a 3-dB bandwidth of 32 GHz through a one meter single modal fiber. Network analyzer ports 1 and 2 are connected to the transmitter signal input and the receiver signal output, respectively. The RF signal power is set to -15 dBm and frequency is swept from 100 MHz to 8.5 GHz. The measured result is shown in Figure 5.5. The result shows the transmitter has 3dB bandwidth greater than 6GHz (around 6.3GHz) and the input impedance is good matched (S11 less than -10dB within this bandwidth), which meets our requirements.

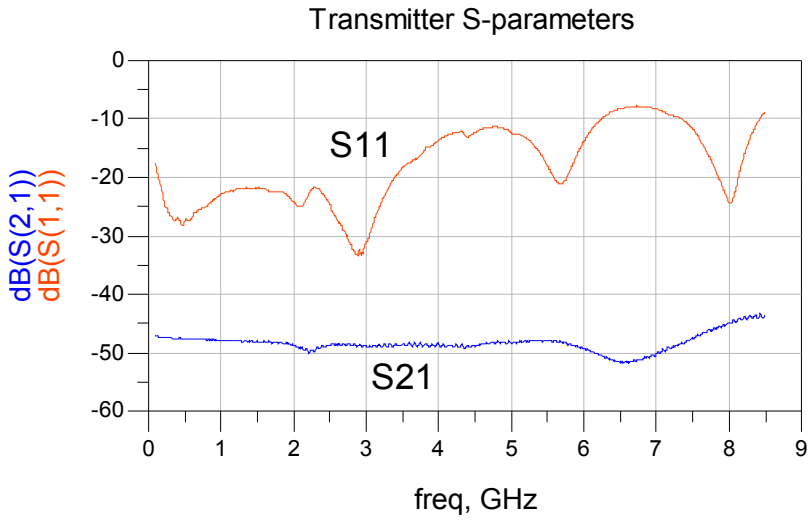

Figure 5.5 Measured TOSA S parameters

5.2 APC Evaluation

Figure 5.6 is the automatic power control (APC) circuit of our transceiver. A NPN BJT provides the current gain to the laser, the R_{FB} resistor provides the feedback voltage of the output optic power, and the MIC3003 controller compare the feedback voltage to the user setup reference voltage to control the BJT. When the temperature increases, the output optic power decreases due to the increases of laser threshold current, so is the photo-detector current and thus the feedback voltage. The controller will then increase the control voltage to increase the bias current and thus the optic power. Constant feedback voltage will indicate constant output optic power. Because it's not convenient to change environment temperature, instead, we varying the feedback resistance to change the feedback voltage which has the equivalent effect with the optic power changing. We measure the bias current and the feedback voltage to see how the system responses.

Figure 5.7 plots the result of 1 watt corresponding reference voltage and varying the feedback resistor from 450 to 1200 ohm, and it clearly shows that when the feedback resistor changes, which means the optic power changes, the bias current will change to compensate the power change and keep the feedback voltage constant, which means keep the output optic power constant.

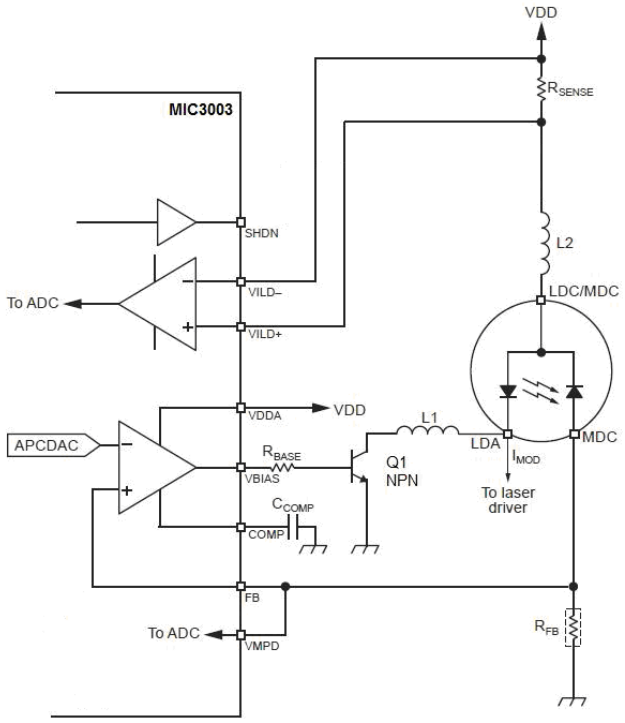

Figure 5.6 APC circuit

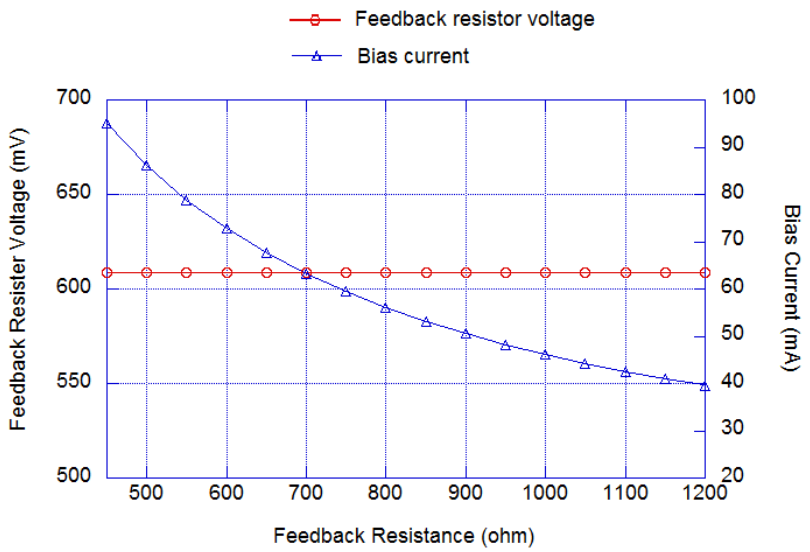

Figure 5.7 Measured feedback resistor voltage and bias current vs. feedback resistance

5.3 Receiver Evaluation

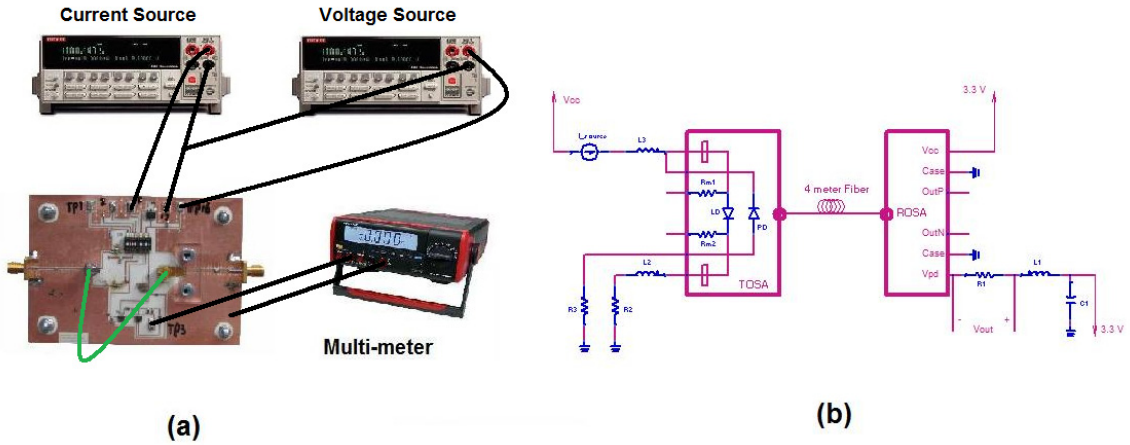

Figure 5.8 ROSA DC evaluation circuit (a) components connection, (b) circuit schematic

The role of the receiver is receiving optic signal and converting it to electric signal and then output it to the external system. Similar as the transmitter, the receiver should be output impedance matched to ensure maximum signal power flow out; within the desired bandwidth, the variation of the gain should be less than 3 dB. Also, a DC and an AC evaluation are conducted for the receiver part of our transceiver. The DC circuit is

constructed as shown in Figure 5.8. The output of the transmitter is connected to the input of the receiver by a four meter single modal fiber. By varying the optic source bias current (as we did in the transmitter DC evaluation), optic power at different levels was sent to the photo-detector, and the performance is evaluated by reading the voltage across the detecting resistor. The result is shown in Figure 5.9. The result shows the I-P curve of the receiver is highly linear with 0.82 mA/mW responsivity.

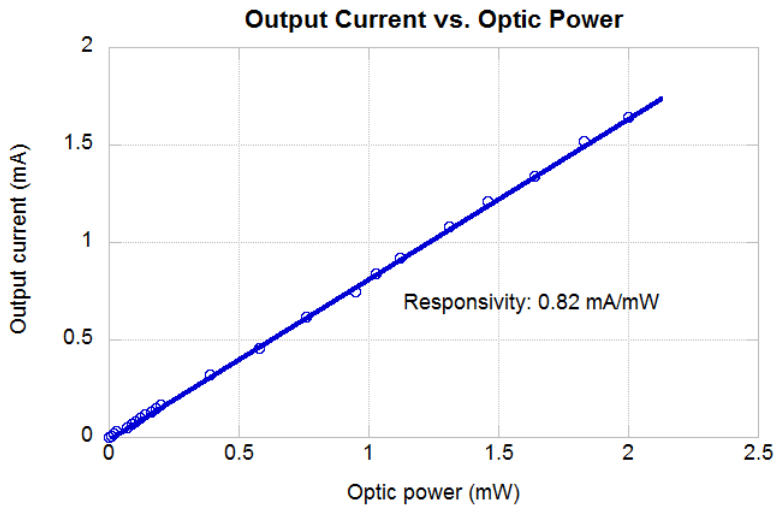

Figure 5.9 Measured ROSA I-P characteristic

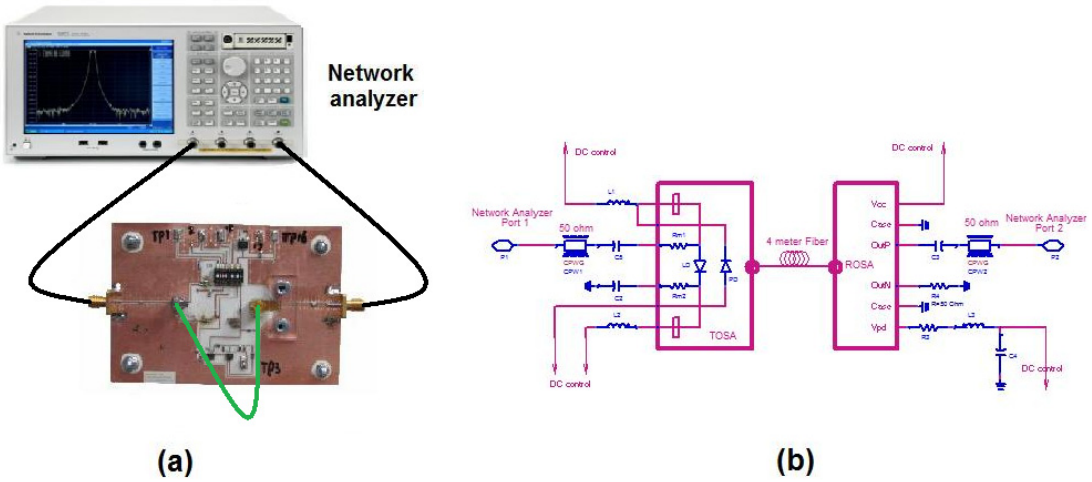

Figure 5.10 Receiver AC evaluation circuit (a) components connection, (b) circuit schematic

The AC performance was conducted by constructing the circuit as shown in Figure 5.10. The output of the transmitter is connected to the input of the receiver by a four meter single modal fiber. Network analyzer ports 1 and 2 are connected to the transmitter signal input and the receiver signal output, respectively. The laser is biased at 50 mA, the RF signal power is set to -15 dBm and the frequency is swept from 100 MHz to 8.5 GHz. Actually, this measurement is not exactly the receiver's performance as it includes the performance of the transmitter as well. To get the performance of the receiver, let's assume in the constructed circuit, Figure 5.11a, an ideal photo-detector, an ideal RF power amplifier, and an ideal laser diode are inserted, as shown in Figure 5.11b. We can see that with proper gain of the RF amplifier, these two circuits will have the same performance. We treat the high-speed optic receiver which was used to evaluate the transmitter in previous section as an ideal photo diode, and then S1 is just the measured S parameter of the transmitter AC performance we got in previous section. So with the S value we measured, we can use the two port network analysis technique to get S2, which

is the performance of the receiver (the S parameters will include the effects of the PA and LD, however, we just interest the 3dB bandwidth, and the exact value is not concerned). The result is plotted in Figure 5.12. We can see that 3dB bandwidth is great than 8GHz and the output impedance is good matched (S22 less than -9.5dB within this bandwidth), which meets our requirements.

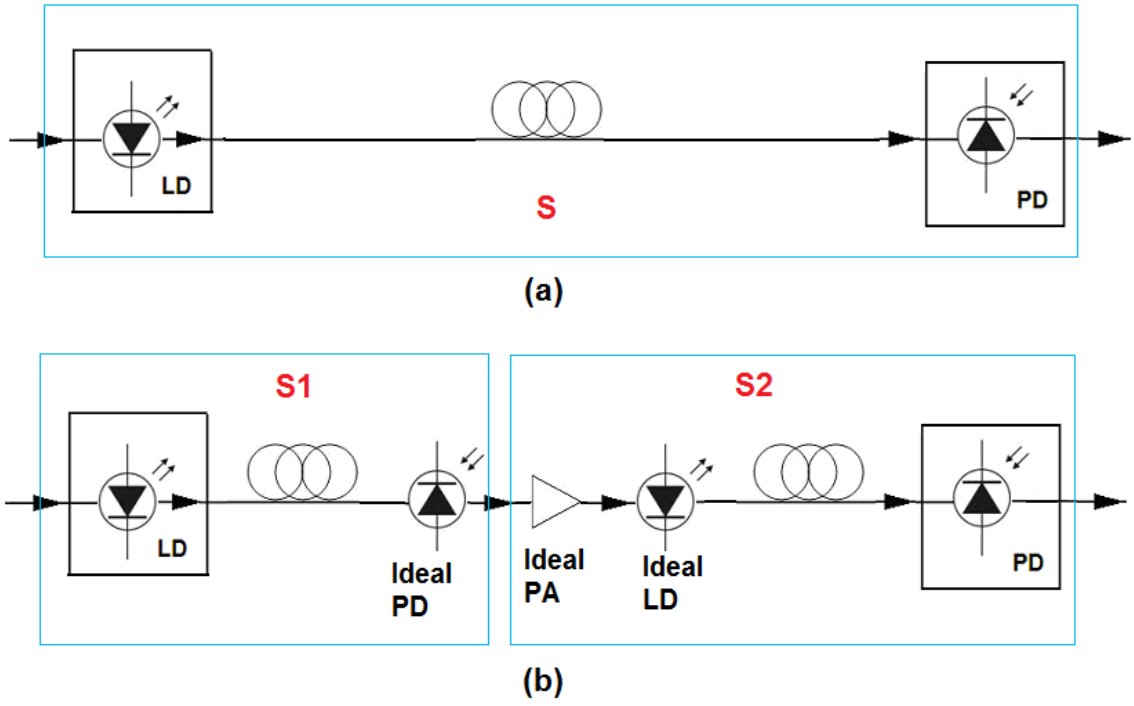

Figure 5.11 Receiver evaluation circuit, (a) simple connection, (b) assume an ideal PD, and ideal PA, and an Ideal LD were inserted in between the transmitter and the receiver.

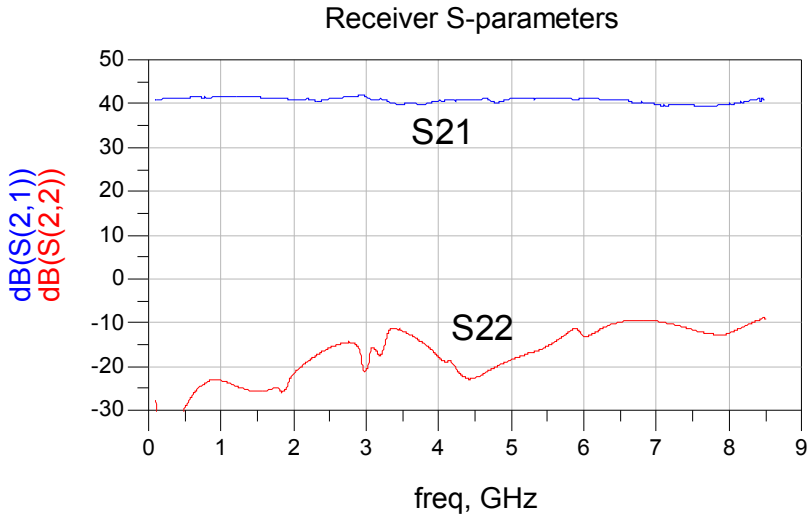

Figure 5.12 Measured Receiver S parameters

5.4 Link S Parameters Evaluation

The circuit in Figure 5.10, which is the receiver AC evaluation circuit, is used to measure the link performance of our transceiver. We use a 4 meter single modal fiber to directly connect the TOSA output and the ROSA input, the laser is controlled to output -1 dBm (0.8 mW) optic power, input RF power is set to -15 dBm and sweep the frequency from 100 MHz to 8.5 GHz. The S parameters measured by the network analyzer are shown in Figure 5.13. This figure indicates that the system gain (S21) is -10 dB and the 3 dB bandwidth is more than 6 GHz, which agrees with our estimations in section 3.6 (-11 dB). Within this band, the input and output impedances are well matched (S11 and S22 both below -12 dB).

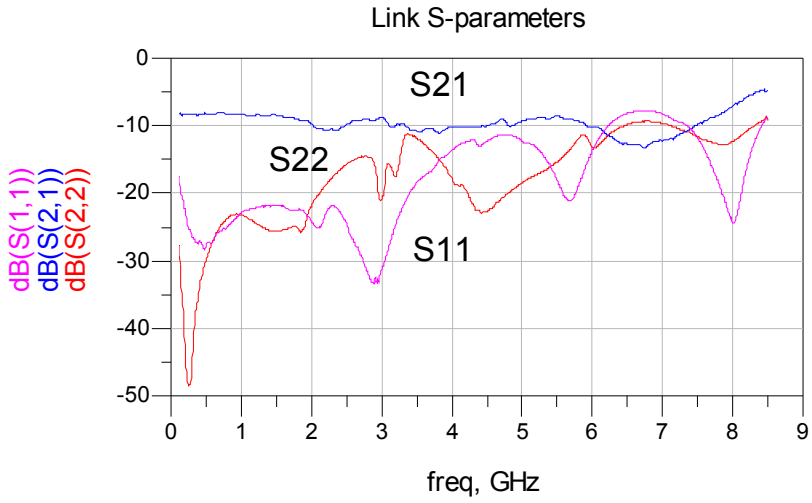

Figure 5.13 Measured Link S parameters

5.5 Link Output P1dB Evaluation

Then we set the frequency at different levels from 100 MHz to 6 GHz, and sweep the input RF power from -20 dBm to 10 dBm. The result gain and the output P1dB are plotted in Figure 5.14 and Figure 5.15, respectively. The results show that the linked system has output P1dB at -9 dBm within 6 GHz band.

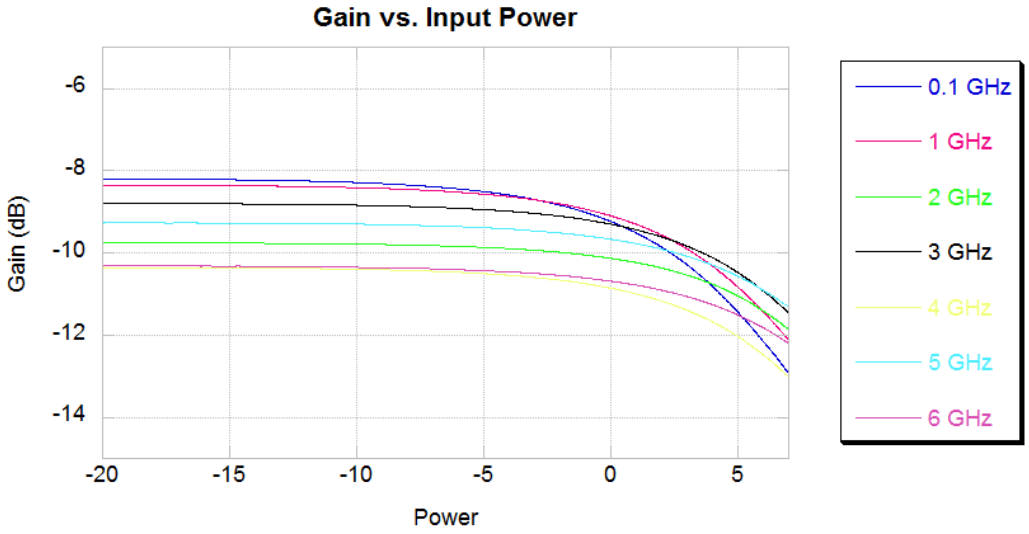

Figure 5.14 Measured Power sweep performance

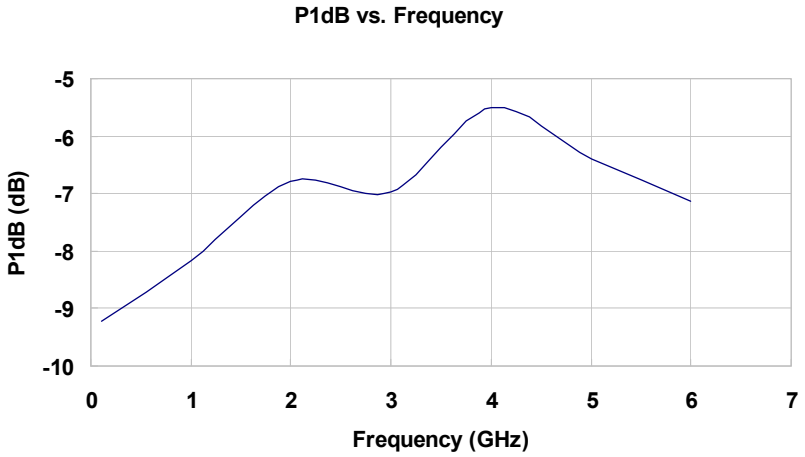

Figure 5.15 Measured Output P1dB

5.6 Link SFDR Evaluation

Spurious Free Dynamic Range (SFDR) is a specification used to characterize the dynamic performance of a system. SFDR specifies the relationship between the amplitude of the fundamental frequency and the amplitude of the most prominent

harmonic.

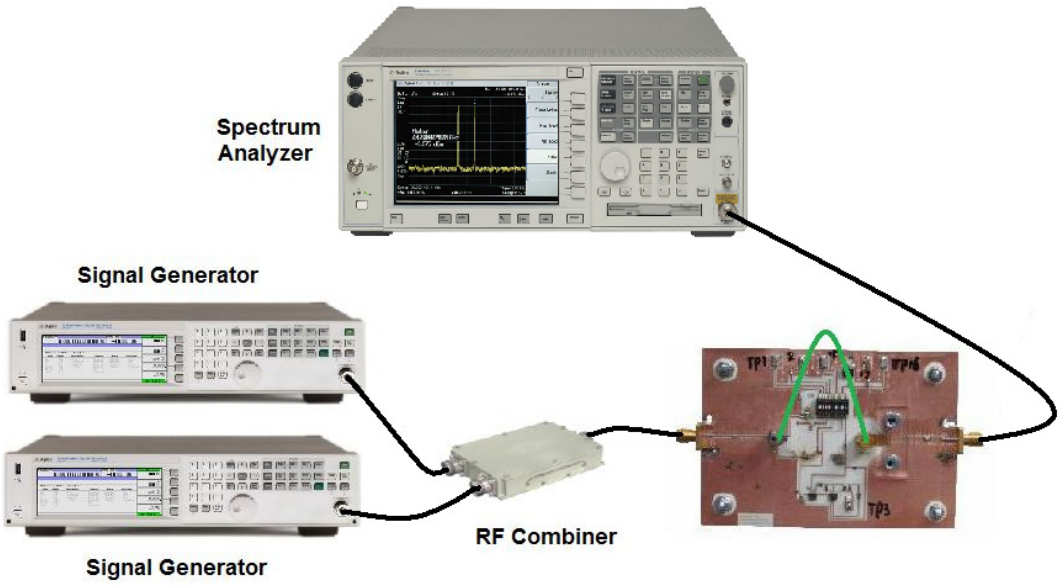

Figure 5.16 Two tone test circuit

Figure 5.16 illustrates the circuit constructed to measure the SFDR. Two signal generators generate two signals at different frequency, and a RF combiner combines these two signals and then inputs to the transceiver. The output signal will be measured by a spectrum analyzer. To find out which distortion will dominant, we chose the two base frequencies as 1.8 and 2.4 GHz. We should expect 2HD at 3.6 and 4.8 GHz, 2 IMD at 0.5 and 4.2 GHz, and 3IMD at 1.2 and 3 GHz. Figure 5.17 shows the output frequency spectrum of these two tone inputs. One can see that the 3IMD is the dominant distortion.

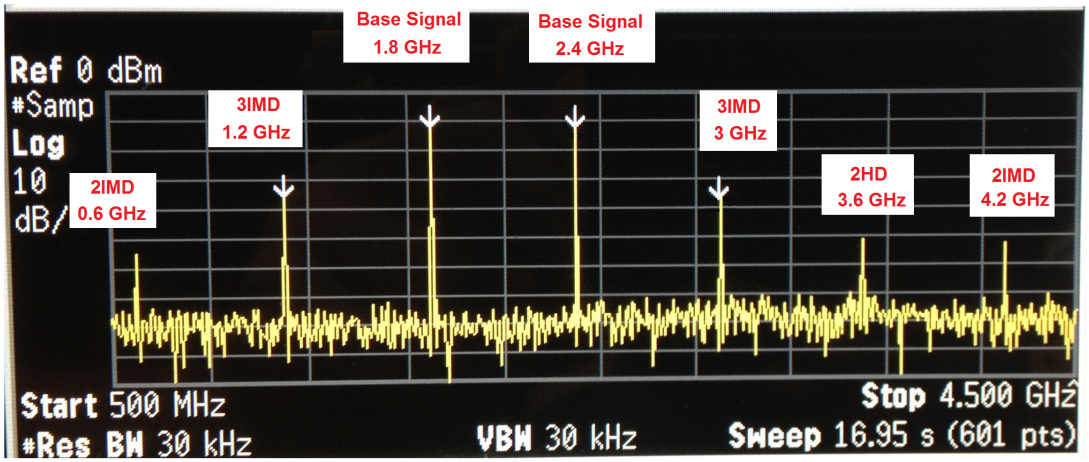

Figure 5.17 Output frequency spectrum for two tones input (1.8 and 2.4 GHz at 0 dBm)

Then we vary the power of these tow tone signals from -10 to 5 dBm and measure the output fundamental signal and the 3IMD, the result is plotted in Figure 5.18. One can find that the output third order intercept point of the transceiver is 10 dBm and the SFDR is 102 dB/Hz$^{2/3}$.

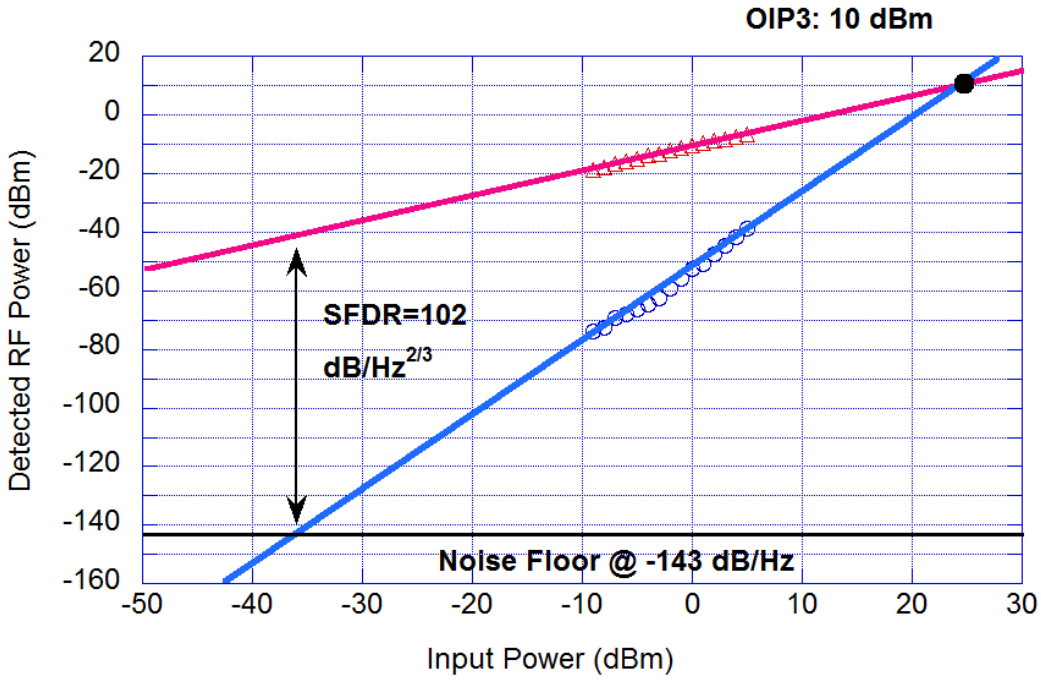

Figure 5.18 Measured OIP3 and SFDR

5.7 UWB OFDM Test

A real application, 20 km transmitting WiMedia Alliance Ultra-Wideband (UWB) orthogonal frequency-division multiplexing (OFDM) signal, is used to evaluate the performance of our system. The UWB OFDM signal consists of 128 subcarriers each has 4.125 MHz and occupying total bandwidth of 528 MHz. Figure 5.19 and Figure 5.20 illustrate UWB band groups and band #1 structure, respectively [23]. Thus the 3IMD is the main distortion when transmitting this signal alone.

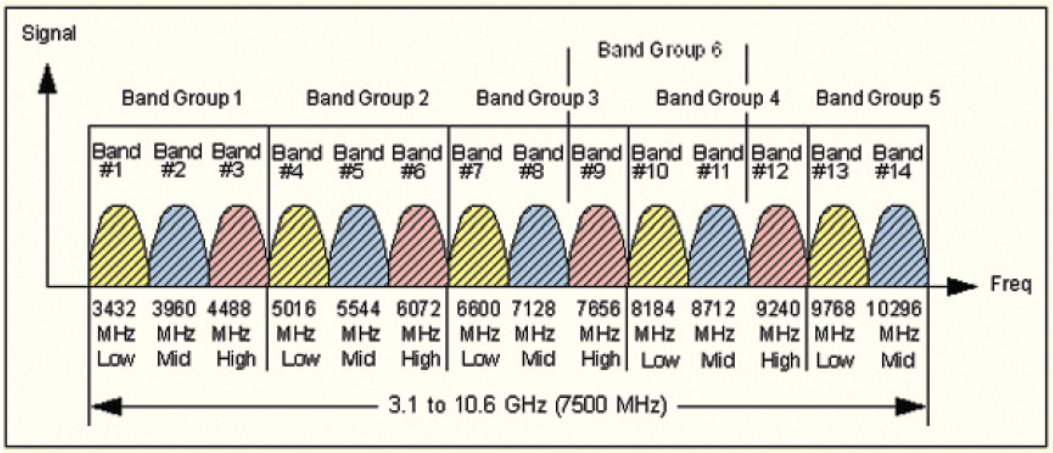

Figure 5.19 Frequency band plan for UWB band groups

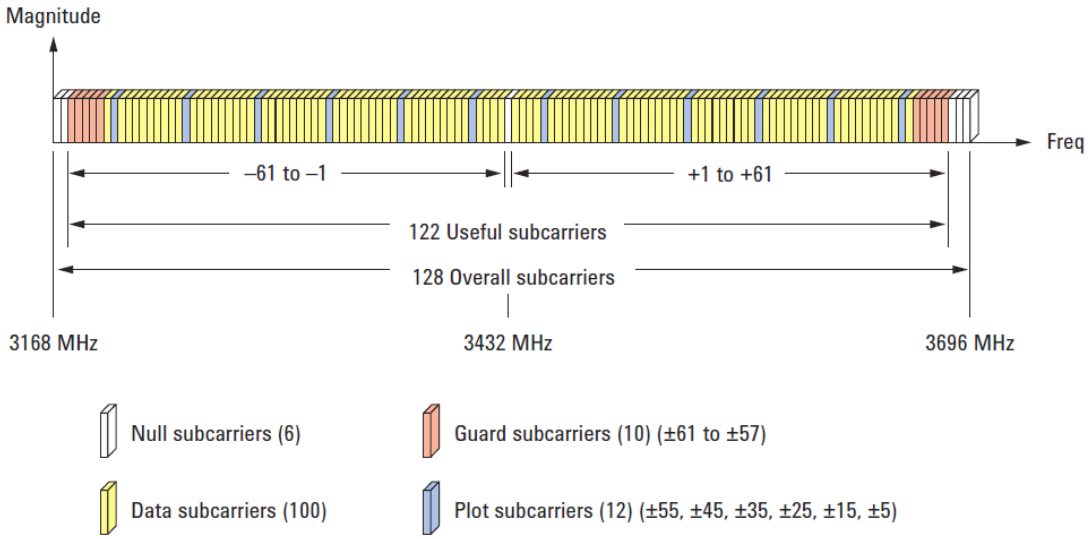

Figure 5.20 Frequency domain structure of UWB OFDM band #1 signal

The experimental setup is shown in Figure 5.21. A 20 km single modal fiber is connected between the optical input and output. The arbitrary wave generator generates the UWB OFDM signal using advanced dual carrier modulation (DCM) technique with bit rate of 480 Mb/s [23]. We measure the error vector magnitude (EVM) of the received OFDM UWB signal using a high speed DSO. The laser is controlled to output -1 dBm optic

power and the signal input power is varied from -14 to 12 dBm using the low noise amplifier (LNA) with a variable RF attenuator (VRA). We did the test for the second WiMedia sub-band allocated at center frequency of 3.96 GHz first, and then the fifth sub-band allocated at center frequency of 5.544 GHz. The measured EVM is shown in Figure 5.22, which indicates that the system has good linearity at the input power between -10 to 9 dBm (EVM is below -18 dB). At high power, through the increase in input power, the third-order inter-modulation distortion increases faster than the signal increases, so the signal to noise ratio decreases, and thus the EVM degrades. We also identify the optimum input power is at around 2 dBm.

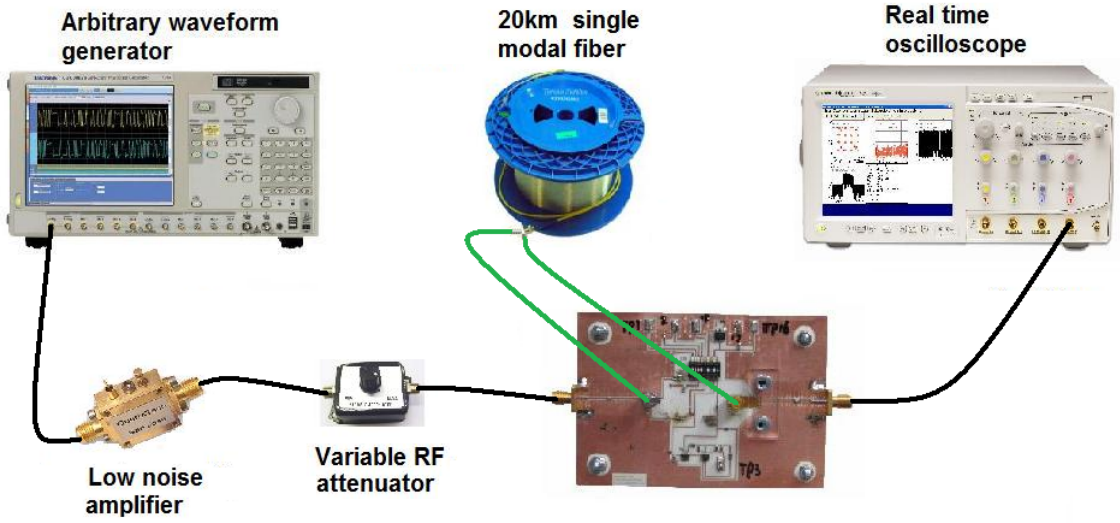

Figure 5.21 OFDM UWB test circuit

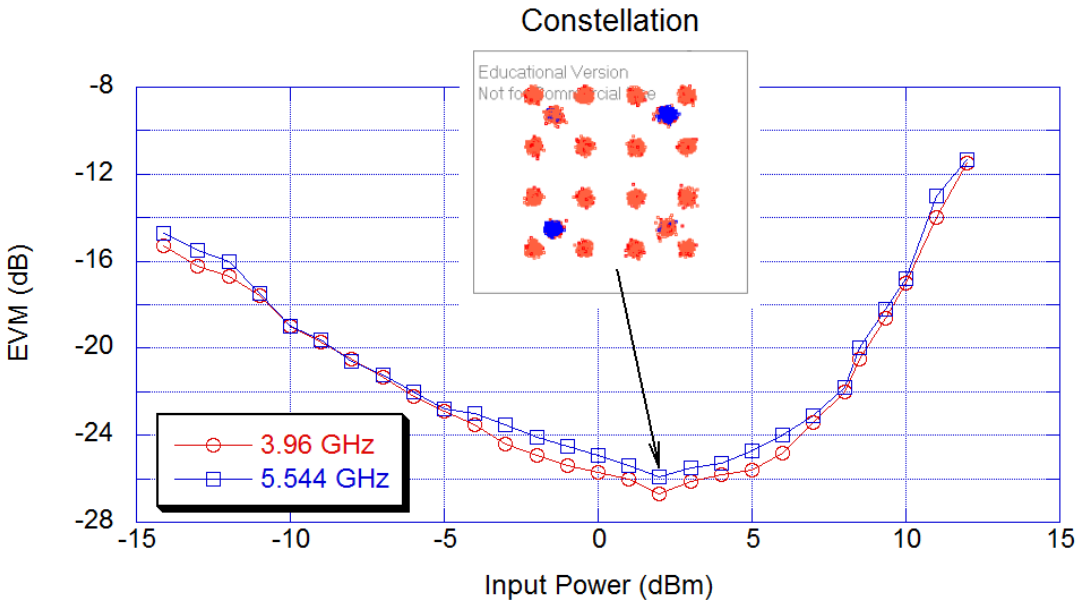

Figure 5.22 Measured EVM vs. Input RF power

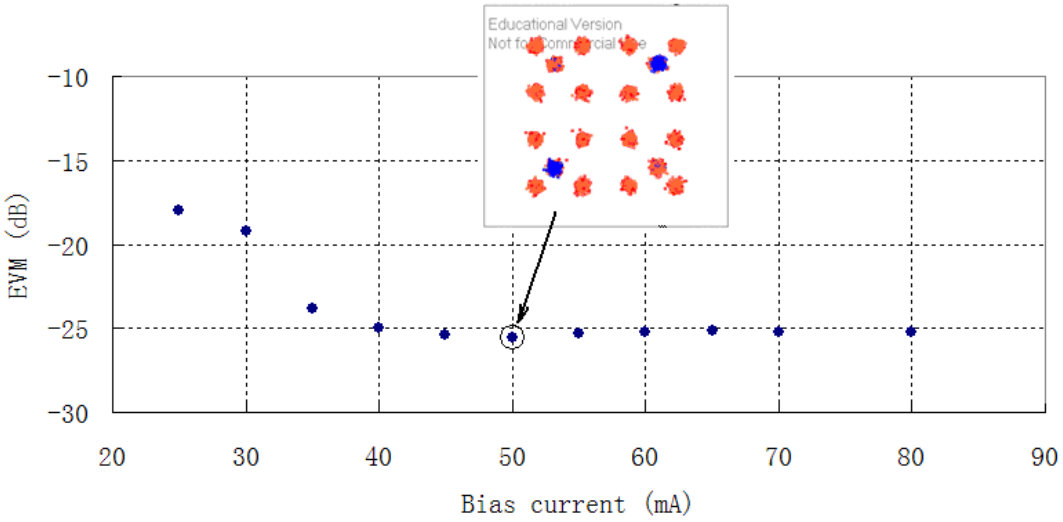

Figure 5.23 Measured EVM vs. Laser bias current

Then we use the 3.96 GHz signal and keep the input power at 2 dBm to find the optimum bias current by varying the bias current from 25 to 80 mA. The result is shown in Figure 5.23. It reveals that the bias current from 40 to 80 mA can give very good performance.

5.8 Multi-Channel Test

We then use multi-channel test to further investigate the transceiver performance when there are 2HD and 3IMD present together. The circuit is the same as in the previous test shown in Figure 5.21. The arbitrary wave generator generates a UWB OFDM signal at center frequency of 3.96 GHz and an interference WiMax signal at 1.98 GHz as shown in Figure 5.24. So the 2HD of the WiMax signal will interfere the UWB signal. First, we varying the UWB signal power and keep the interference signal always 3 dB greater than the UWB signal, the measured EVM for received UWB signal and the result from last test without the interference signal are plotted in Figure 5.25. Then we keep the UWB signal as -6 dBm and increase the interference signal power gradually and then measure the EVM and plotted in Figure 5.26. These two diagrams clearly demonstrates that only when the interference signal has the power around 20 dB greater than the UWB signal, the 2HD will affects its performance.

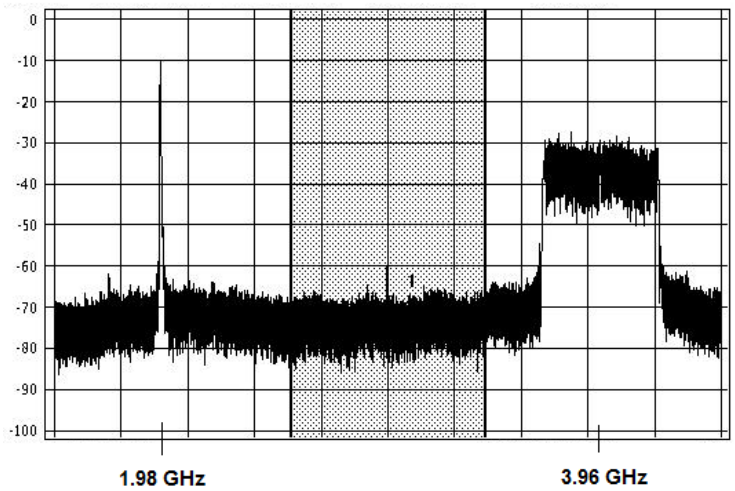

Figure 5.24 Spectrum of 3.96 GHz OFDM UWB signal and 1.98 GHz WiMax interference signal

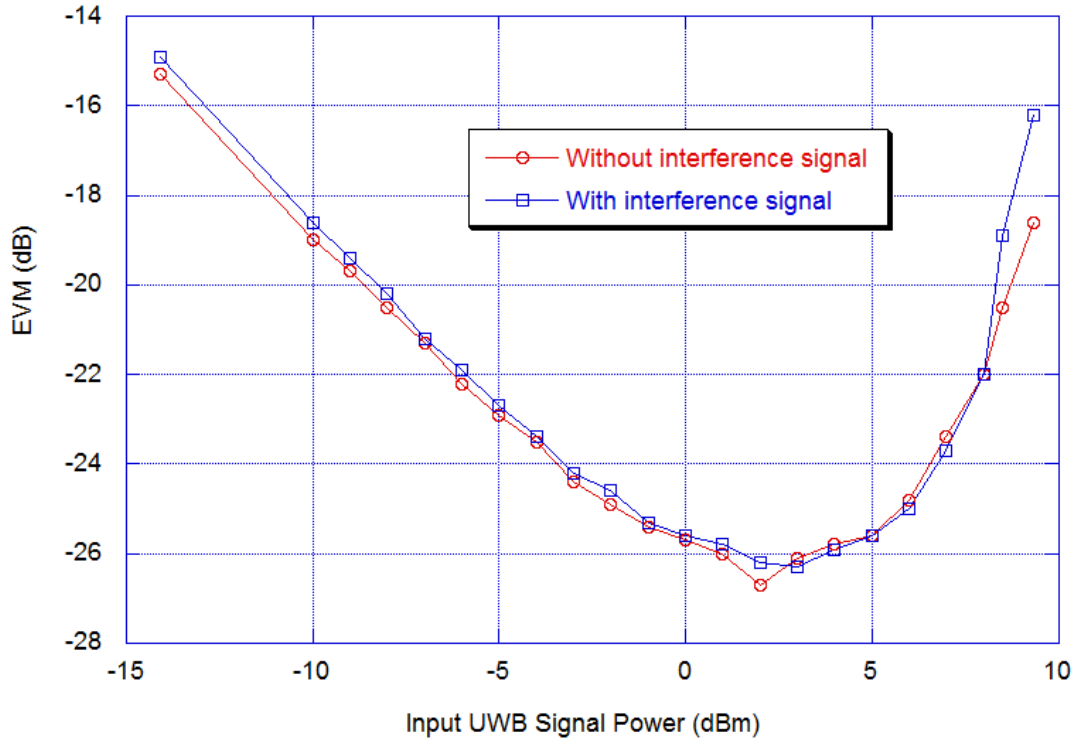

Figure 5.25 Measured EVM of OFDM signal with and without interference signal

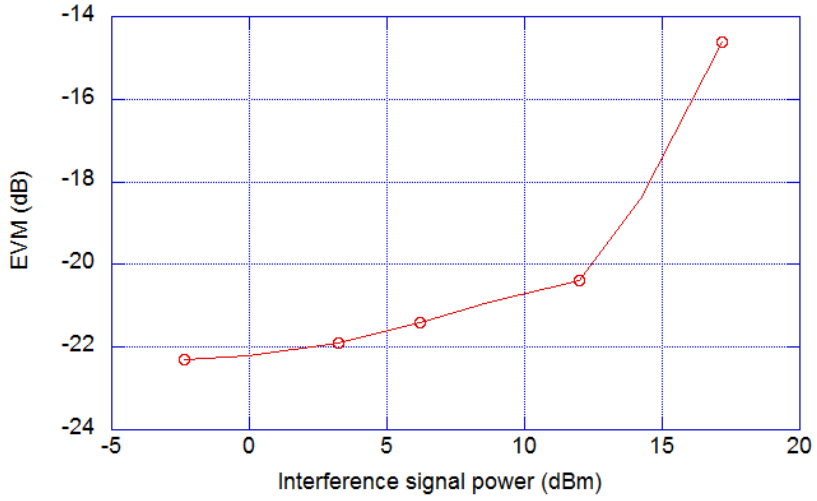

Figure 5.26 Measured EVM vs. interference signal power at -6 dBm UWB signal power

5.9 Product Specification

Based on the experiment results, we get the system specification as shown in Table 5-1.

Table 5-1 Transceiver specification

Parameters	Value	Unit	Notes
Reach distance	20	Km	
Operation wave length	1295 ~ 1315	nm	
Spectral width	1.4	nm	
Link gain	-10	dB	
3 dB frequency range	0.1 ~ 6	GHz	
Link noise figure	31	dB	
Link OIP3	10	dBm	
Link OP1dB	-9	dBm	
Link SFDR	102	$dB/Hz^{2/3}$	
Input RF power range	-10 ~ 9	dBm	
RF input return loss	12	dB	
RF output return loss	12	dB	
Laser operation current	40 ~ 80	mA	
Laser output power	0.6 ~ 1.3	mW	At specified operation current
Laser slope efficiency	0.0175	mW/mA	
PD responsivity	0.82	mA/mW	
Maximum PD input	2	mW	
Operation temperature	-10 ~ 85	ºC	
Storage temperature	-40 ~ 85	ºC	
RF connector	SMA		
Optical connector	LC		
Supply voltage	5	V	

CHAPTER 6 CONCLUSION

The thesis has been focused on the design and implementation of a cost effective direct modulation 20 km reach optical transceiver working from 100 MHz to 6GHz. The detailed theoretical analysis of the transceiver design has been presented, and the power budget analysis, bandwidth budget analysis, noise analysis, linearity analysis, and economic consideration have jointly justified the design of the proposed transceiver. The analysis results are verified by comparing the calculation results with simulations and measurements. Through carefully evaluating the product with AC and DC test for both transmitter and receiver, link S parameter and P1dB measurement, link two tone test, and single and multi-channel OFDM UWB signal over 20 km of fiber transmission, the thesis proves that this transceiver exhibits more than 6 GHz 3-dB gain bandwidth with -10 dB link gain and very good match at its input and output impedances, 31 dB link noise figure, -9 dBm output P1dB, 10 dBm OIP3 and 102 dB SFDR.

The proposed 6 GHz 20 Km reach optical analog transceiver is a feasible and optimal option for OFDM UWB RoF systems. That being said, it also implies significant room for improvement. There will be some future researches on the transceiver design in terms of the following aspects:

- From the system specification provided in previous Chapter, one can see that the maximum output optic power is low (around 3 dBm) which limit the maximum input signal power. Also the link gain of the system is -10 dB, which is considered small

and limits the minimum input signal power. This gain depends on the laser slop efficiency and photo-detect responsivity and current gain. The photo-detect responsivity of our photo-detector is 0.82 mA/mW, which is normal value, and we don't want to use an APD photo-detector to increase the operation voltage as well as the related cost. So the only way is to choose higher slop efficiency laser, where double the laser slop efficiency will obtain 4 times increase for the link gain. Our laser slop efficiency is 0.0175 mW/mA, which is very small (normal laser can achieve 0.3 mW/mA). We will keep searching the market to find satisfactory laser with higher output power and higher slop efficiency to improve our system link gain.

- Optimize the size of the transceiver. In this thesis, we separate the transceiver circuit into two parts, and there are many components used for easy testing and debugging, so the size of this product is much larger than the products on the market. After verification, some components can be removed and the rest components can be compressed into one PCB and packed into a shielding box.

- Design an adapter for LC receptacle and LC connector. In the transceiver, we choose TOSA and ROSA with LC receptacle interface, and this interface should work with the LC connector. However, from Figure 6.1, one can see that the LC connector can connect to the receptacle, but there is no mechanism to hold it. As a matter of fact, we handheld the LC connector and the receptacle to finish the measurement. We contacted many big optical connector manufacturers and they don't provide such an adapter which can hold LC receptacle and connector. Since both receptacle and

connector are standard and popular products, this adapter should also have significant market potential.

Figure 6.1 LC receptacle and LC connector

APPENDIX A: 6 GHZ 30DB GAIN 1 WATT POWER AMPLIFIER

Circuit layout

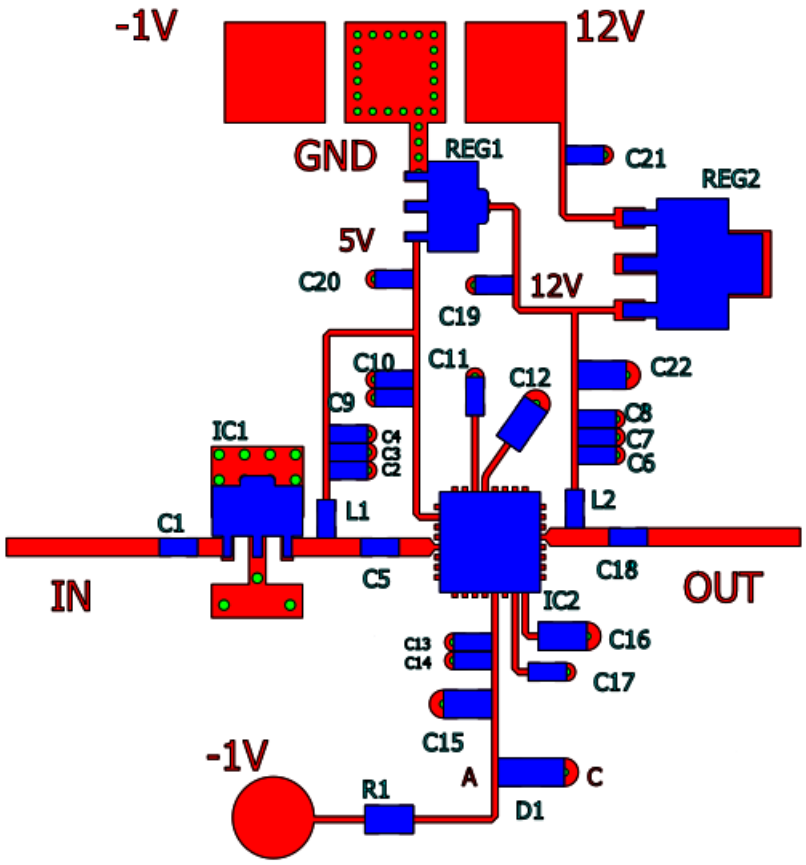

Components list

Capacitor			
Value	Size	Manufacturer Part No.	Circuit symbol
68 pf	0603	GRM1885C1H680JA01D	C2,C6
100 pf	0603	GRM1885C1H101JA01D	C1,C5,C9,C13,C18
1000 pf	0603	GRM1885C1H102JA01D	C10,C11,C14,C17
1200 pf	0603	GRM1885C1H122JA01D	C3,C7
1 uf	0603	GCM188R71C105KA64D	C4,C8,C19,C20
0.47 uf	0603	GCM188R71C474KA55D	C21
4.7 uf	0805	GRM21BR61E475KA12L	C12,C15,C16
22 uf	0805	C2012X5R1C226K	C22

Inductor			
Value	Size	Manufacturer Part No.	Circuit symbol
39 nH	0603	LQW18AN39NJ00D	L1, L2

Resistor			
Value	Size	Manufacturer Part No.	Circuit symbol
49.9 ohm	0805	MCR10EZPF49R9	R1

Amplifier IC	
Manufacturer Part No.	Circuit symbol
HMC637LP5	IC_2
SBB5089Z	IC_1

SMA connector	
Manufacturer Part No.	Quantity
142-0701-631	2

221108-4	10

Voltage Regulator			
Value	Size	Manufacturer Part No.	Circuit symbol
5 V	SOT89	MCP1702T-5002E/MB	REG1
12 V	SOT223	LM2940IMP-12/NOPB	REG2

Zener Diode			
Value	Size	Manufacturer Part No.	Circuit symbol
2.2 V	1005	CZRF52C2V2	D1

Heat Sink	
Manufacturer Part No.	Quantity
ATS-54450W-C2-R0	1

Substrate: RO4350B 16.6mil

Final product

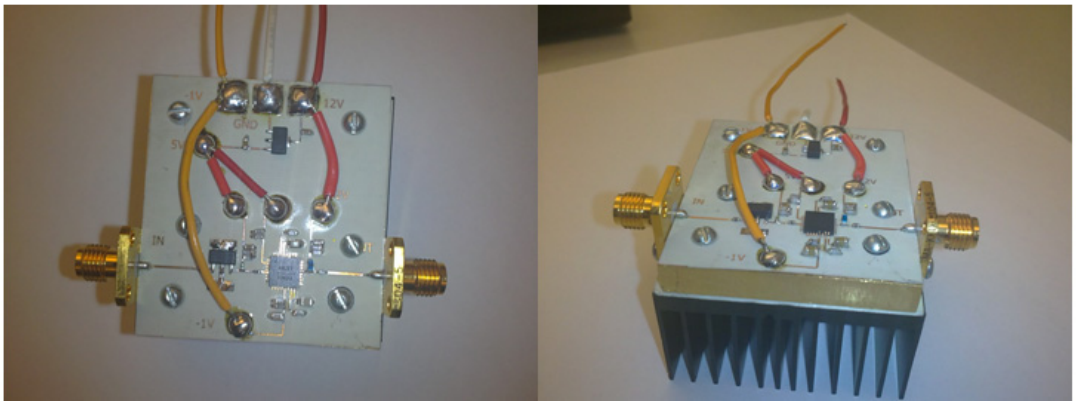

System specification

Parameter	Typical Value	Units
Frequency Range	0.1 ~ 6	GHz
Gain	33.5 (@ 500MHz)	dB
	29 (@ 5GHz)	dB
Input return loss (maximum)	-8	dB
Output return loss (maximum)	-10	dB
OIP3	40	dBm
Output P1dB	30	dBm
Noise figure	4.3	dB
Supply voltage	12 and -1	V
Supply current	500	mA

APPENDIX B: TRANSCEIVER CIRCUITS SCHEMATIC AND COMPONENTS LIST

Schematic of AC circuit

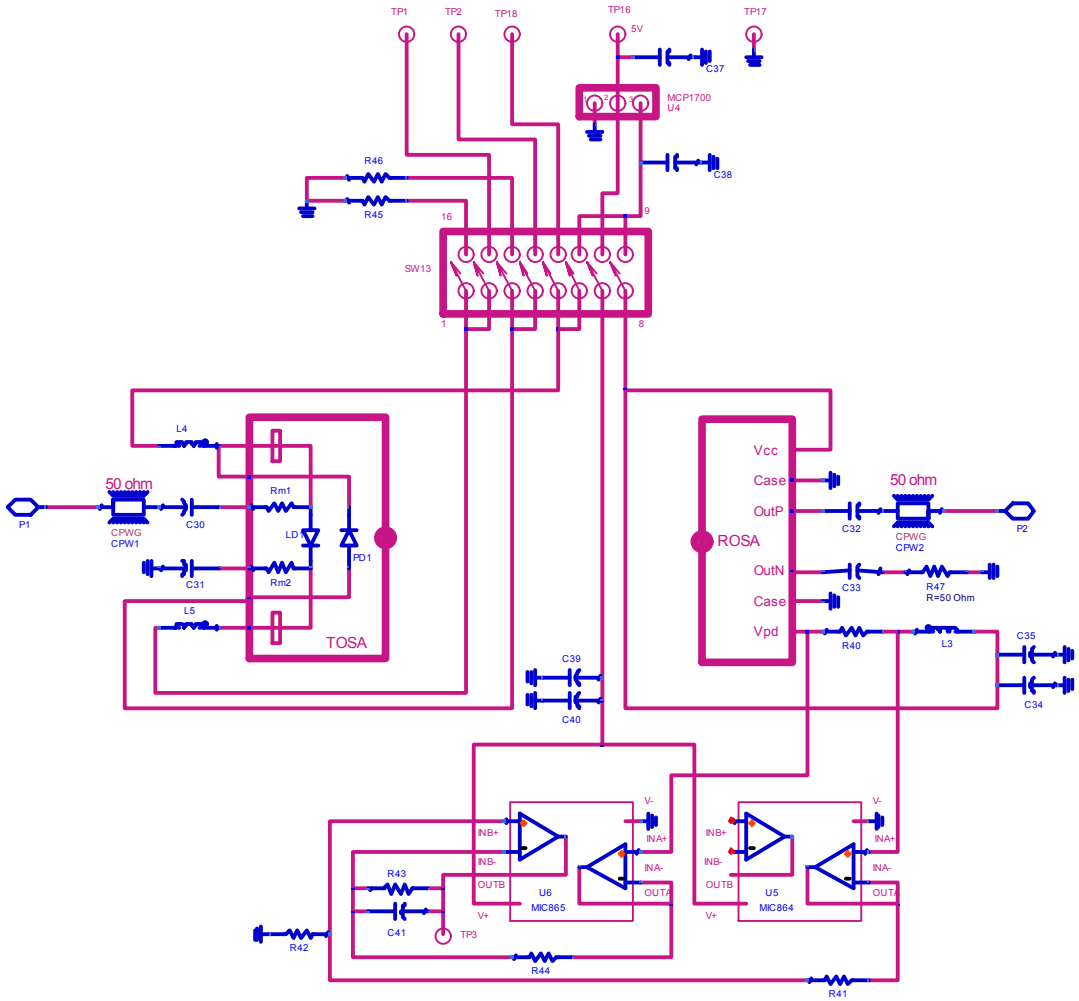

Schematic of DC circuit

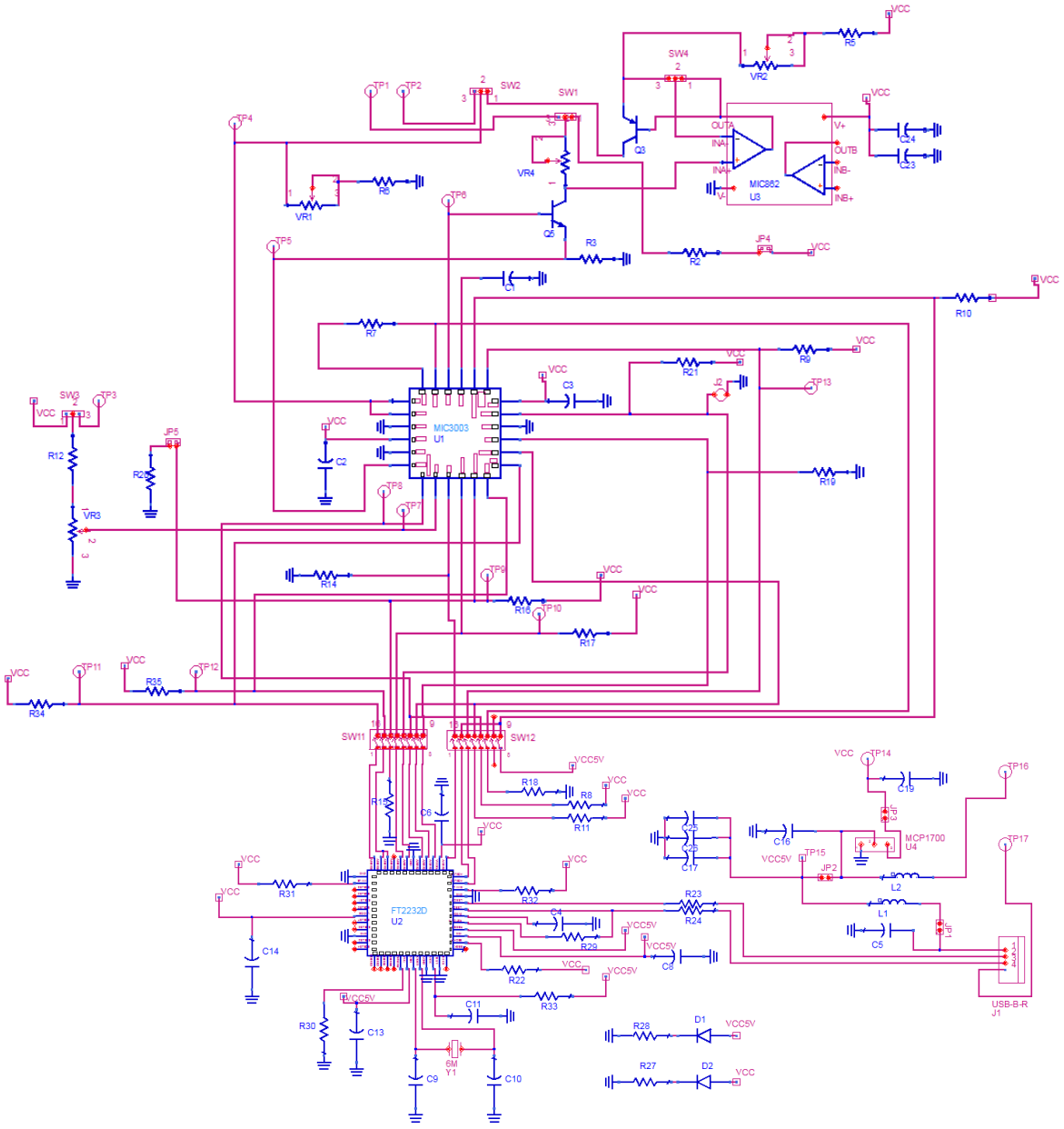

Transceiver circuit components list

ICs			
Symbol	Value	Size	Manufacturer Part No.
TOSA			FP-1310-10LRM-LCA
ROSA			PIN-1310-10LR-LC
REG1	3.3 V	SOT89	MCP1700T-3302E/MB
REG2	3.3 V	SOT89	MCP1700T-3302E/MB
U2	USB to serial		FT2232D-REEL
U1	LASER controller		MIC3003GML
U3	OPAMP		MIC862YM8 TR
U4	OPAMP		MIC862YM8 TR
U5	OPAMP		MIC862YM8 TR
Y1	6M CRYSTAL		ABMM-6.000MHZ-B2-T
Q1	NPN transistor		MMBT3904WT1G
Q2	PNP transistor		MMBT3906WT1G

Capacitor			
Symbol	Value	Size	Manufacturer Part No.
C1	0.018 uf	0603	GRM188R71H183KA01D
C2	0.1 uf	0603	GRM188R71H104KA93D
C3	0.1 uf	0603	GRM188R71H104KA93D
C4	0.033 uf	0603	GRM188R71H333KA61D
C5	0.01 uf	0603	GRM188R71H103KA01D
C6	0.01 uf	0603	GRM188R71H103KA01D
C8	0.1 uf	0603	GRM188R71H104KA93D
C9	18 pf	0603	GRM1885C1H180JA01D
C10	18 pf	0603	GRM1885C1H180JA01D
C11	0.1 uf	0603	GRM188R71H104KA93D
C13	0.1 uf	0603	GRM188R71H104KA93D
C14	0.01 uf	0603	GRM188R71H103KA01D
C16	1.0 uf	0603	GRM188R61E105KA12D
C17	10 uf	1206	TAJA106K016RNJ
C19	1.0 uf	0603	GRM188R61E105KA12D
C20	1.0 uf	0603	GRM188R61E105KA12D
C21	1.0 uf	0603	GRM188R61E105KA12D

C22	1.0 uf	0603	GRM188R61E105KA12D
C23	0.1 uf	0603	GRM188R71H104KA93D
C24	10 uf	0603	GRM188R60J106ME47D
C25	0.1 uf	0603	GRM188R71H104KA93D
C26	0.1 uf	0603	GRM188R71H104KA93D
C30	100 pf	0603	GRM1885C1H101JA01D
C31	100 pf	0603	GRM1885C1H101JA01D
C32	100 pf	0603	GRM1885C1H101JA01D
C33	100 pf	0603	GRM1885C1H101JA01D
C34	100 UF	1206	GRM31CF50J107ZE01L
C35	0.1 uf	0603	GRM188R71H104KA93D
C36	1.0 uf	0603	GRM188R61E105KA12D
C37	1.0 uf	0603	GRM188R61E105KA12D
C38	1.0 uf	0603	GRM188R61E105KA12D
C39	10 uf	0603	GRM188R60J106ME47D
C40	0.1 uf	0603	GRM188R71H104KA93D
C41	1.0 uf	0603	GRM188R61E105KA12D

Inductor			
Symbol	Value	Size	Manufacturer Part No.
L1,L2	1.2 uH	1008	FSLU2520-1R2JP2
L3	100 nH	0603	LQW18ANR10J00D
L4	100 nH	0603	LQW18ANR10J00D
L5	100 nH	0603	LQW18ANR10J00D

Resistor			
Symbol	Value (ohm)	Size	Manufacturer Part No.
R2	10	0603	CRCW060310R0FKEA
R3	3.3	0603	CRCW06033R30FKEA
R5	10	0603	CRCW060310R0FKEA
R6	10	0603	CRCW060310R0FKEA
R7	10 k	0603	CRCW060310K0FKEA
R8	10 k	0603	CRCW060310K0FKEA
R9	10 k	0603	CRCW060310K0FKEA
R10	10 k	0603	CRCW060310K0FKEA

R11	10 k	0603	CRCW060310K0FKEA
R12	10 k	0603	CRCW060310K0FKEA
R14	100	0603	CRCW0603100RFKEA
R15	100	0603	CRCW0603100RFKEA
R16	10 k	0603	CRCW060310K0FKEA
R17	10 k	0603	CRCW060310K0FKEA
R18	10 k	0603	CRCW060310K0FKEA
R19	100	0603	CRCW0603100RFKEA
R20	100	0603	CRCW0603100RFKEA
R21	10 k	0603	CRCW060310K0FKEA
R22	1.5 k	0603	CRCW06031K50FKEA
R23	27	0603	CRCW060327R0FKEA
R24	27	0603	CRCW060327R0FKEA
R27	270	0603	CRCW0603270RFKEA
R28	270	0603	CRCW0603270RFKEA
R29	1.5 k	0603	CRCW06031K50FKEA
R30	1 k	0603	CRCW06031K00FKEA
R31	10 k	0603	CRCW060310K0FKEA
R32	10 k	0603	CRCW060310K0FKEA
R33	470	0603	CRCW0603470RFKEA
R34	10 k	0603	CRCW060310K0FKEA
R35	10 k	0603	CRCW060310K0FKEA
R36	40.2 k	0603	CRCW060340K2FKEA
R40	100	0603	CRCW0603100RFKEA
R41	1.5 k	0603	CRCW06031K50FKEA
R42	30 k	0603	CRCW060330K0FKEA
R43	30 k	0603	CRCW060330K0FKEA
R44	1.5 k	0603	CRCW06031K50FKEA
R45	27	0603	CRCW060327R0FKEA
R46	1.5 k	0603	CRCW06031K50FKEA
R47	49.9	0805	MCR10EZPF49R9
VR1 to VR4	50k Variable Resistor		3269W-1-503LF
D1,D2	Led		HSMG-C190

Others			
Symbol	Value	Size	Manufacturer Part No.

SW11,SW12	8-position switch		TDA08H0SB1
J1	USB connector		670688010
TP1 to TP17	Test point yellow		5014
JP1 to JP5	Connector header 2 position		3-644456-2
SW1 to SW4	Connector header 3 position		3-644456-3
SW13	8-position switch		TDA08H0SB1
SMA1, SMA2	SMA connector		142-0701-801
TP1,2,3,16,17,18	Test point surface mount		5016

REFERENCE

[1] Gerd Keiser, "Optical Fiber Communications", McGraw-Hill, 1991, pp. 357.

[2] T. Darcie and G. Bodeep, "Lightwave subcarrier CATV transmission systems," IEEE Trans. Microw. Theory Tech., vol. 38, no. 5, pp. 524–533, May 1990.

[3] A. Seeds, "Microwave photonics," IEEE Trans. Microw. Theory Tech., vol. 50, no. 3, pp. 877–887, Mar. 2002.

[4] H. Lu, W. Tsai, A.S. Patra, S. Tzeng, H. Peng, H. Ma, "CATV/ROF transport systems based on -1 side mode injection-locked and optoelectronic feedback techniques," *J. Optics A: Pure and Applied Optics,* vol. 10, no. 5, May 1, 2008.

[5] Y. Chung, K. Choi, J. Sim, H. Yu, J. Kim, " A 60-GHz-band analog optical system-on-package transmitter for fiber-radio communications," *J. Lightw. Technol*., vol. 25, no.11, pp. 3407-3412, Nov. 2007.

[6] Y. Chi, H. Lu, P. Lai, H. Yee, S. Tzeng, "CATV/ROF transport systems based on light injection/optoelectronic feedback techniques and photonic crystal fiber," in *2007 Conference on Lasers and Electro Optics and the Pacific Rim Conference on Lasers and Electro-Optics*, pp. 495-496, 2008.

[7] H. Kim, J. M. Cheong, C. Lee, and Y. C. Chung, "Passive optical network for microcellular CDMA personal communication service*," IEEE Photonics Tech. Lett*., vol. 10, no. 11, pp. 1641-1643, Nov. 1998.

[8] H. Al-Raweshidy, S. Komaki, Radio over fiber technologies for mobile communication networks, 1st ed., 2002, Boston: Artech House.

[9] Ng'oma, "Radio-over-Fibre Technology for Broadband Wireless Communication Systems," Ph.D. thesis, Electrical Engineering, Eindhoven Univ., 2005, page 19.

[10] Eduard Sackinger, "Broadband Circuits for Optical Fiber Communication", WILEY & SONS, 2005, page 234.

[11] Govind P. Agrawal, "Fiber-Optic Communication Systems", JOHN WILEY & SONS, 2002, page 112

[12] Joseph C. Palais, "Fiber Optic Communications", Pearson Prentice Hall, 2005, page 192-194

[13] Eduard Sackinger, "Broadband Circuits for Optical Fiber Communication", WILEY & SONS, 2005, page 250,251.

[14] Joseph C. Palais, "Fiber Optic Communications", Pearson Prentice Hall, 2005, page 219

[15] Joseph C. Palais, "Fiber Optic Communications", Pearson Prentice Hall, 2005, page 399

[16] Joseph C. Palais, "Fiber Optic Communications", Pearson Prentice Hall, 2005, page 401

[17] Govind P. Agrawal, "Fiber-Optic Communication Systems", JOHN WILEY & SONS, 2002, page 39

[18] Joseph C. Palais, "Fiber Optic Communications", Pearson Prentice Hall, 2005, page 113

[19] Govind P. Agrawal, "Fiber-Optic Communication Systems", JOHN WILEY & SONS, 2002, page 42

[20] Gerd Keiser, "Optical Fiber Communications", McGraw-Hill, 1991, pp. 358-361

[21] Govind P. Agrawal, “Fiber-Optic Communication Systems”, JOHN WILEY & SONS, 2002, page 114

[22] Joseph C. Palais, “Fiber Optic Communications”, Pearson Prentice Hall, 2005, page 358-385

[23] http://www.ieee802.org/15/pub/2003/Jul03/03268r2P802-15_TG3a-Multi-band-CFP-Document.pdf [Online].

[24] Govind P. Agrawal, “Fiber-Optic Communication Systems”, JOHN WILEY & SONS, 2002, page 39

[25] Eduard Sackinger, “Broadband Circuits for Optical Fiber Communication”, WILEY & SONS, 2005, page 282.

[26] R. Sadhwani, and Bahram, “Adaptive CMOS predistortion linearizer for fiber-optic links,” J. Lightw. Technol., vol. 21, no. 12, pp. 3180-3193, Dec. 2003.

[27] H. Jung, G. Lee, S. Han, and W. Choi, “Nonlinearity suppression of electroabsorption modulator through dual-parallel modulation,” Microwave Opt. Technol. Lett. , vol. 29, no. 1, pp. 2-5, Apr. 2001.

[28] B. Masella, B. Hraimel, and X. Zhang, “Enhanced spurious-free dynamic range using mixed polarization in optical single sideband Mach-Zehnder modulator,” J. Lightw. Technol., vol. 27, no. 15, pp. 3034-3041, Aug. 2009.

[29] T. Iwai, K. Sato and K. Suto, “Signal distortion and noise in AM-SCM transmission systems employing the feedforward linearized MQW-EA external modulator,” J. Lightw. Technol., vol. 13, no. 8, pp. 1606-1612, Aug. 1995.

[30] S. Sohn, and S. Han, "Linear optical modulation in serially cascaded electroabsorption modulator," Microwave Opt. Technol. Lett. , vol. 27, no. 6, pp. 447-450, Dec. 2001.

[31] G. C. Wilson, T. H. Wood, M. Gans, J. L. Zyskind, J. W. Sulhoff, J. E. Johnson, T. Tanbun-Ek, and P. A. Morton, "Predistortion of electroabsorption modulators for analog CATV systems at 1.55μm," J. Lightw. Technol, vol. 15, no. 9, pp. 1654-1662, Sep.1997.

[32] L. Roselli, V. Borgioni, F. Zepparelli, F. Ambrosi, M. Comez, P. Faccin, and A. Casini, "Analog laser predistortion for multiservice radio-over-fiber systems," J. Lightw. Technol., vol. 21, no. 5, pp. 1211-1221, May 2003.

[33] H. Lu, S. Tzeng, and Y. Liu, "Intermodulation distortion suppression in a full-duplex radio-on-fiber Ring Networks," IEEE Photon. Tech. Lett., vol.16, no.2, pp. 602-604, Feb. 2004.

[34] V. J. Urick, M. S. Rogge, P. F. Knapp, L. Swingen, and F. Bucholtz, "Wideband predistortion linearization for externally modulated long-haul analog fiber-optic links," IEEE Trans. Microwave. Theory Tech., vol. 54, no. 4, April 2006.

[35] N. Imai, T. Nojima and T. Murase, "Novel linearizer using balanced circulators and its application to multilevel digital radio systems," IEEE Trans. Microwave. Theory Tech, vol.37, no.8, pp. 1237-1243, Aug. 1989.

[36] S. C. Bera, R. V. Singh, and V. K. Grag, "Diode-based predistortion linearizer for power amplifier," Electron. Lett., vol.44, no. 2, pp. 125-126, Jun. 2008.

[37] H. Jeong, S. Park, N. Ryu, Y. Jeong, I. Yom, and Y. Kim, "A design of K-band predistortion linearizer using reflective schottky diode for satellite TWTAs," in 13th GAAS Symposium, pp. 597-600, 2005.

[38] L. Roselli, V. Borgioni, V. Palazzari, F. Alimenti, "An active cuber circuit for power amplifier analog predistortion," in 33rd European Microwave Conference, pp. 1219-1222, 2003.

[39] H. Park, S. Jung, K. Lim, M. Kim, H. Kim, C. Park and Y. Yang, "Analysis and design of compact third-order intermodulation generation circuits," Microwave Opt. Technol. Lett. , vol. 51, no. 9, pp. 2137-2140, Sep. 2009.

[40] Eduard Sackinger, "Broadband Circuits for Optical Fiber Communication", WILEY & SONS, 2005, page 290-293.

[41] D. Hassin and R. Vahldieck. Feedforward linearization of analog modulated laser diodes: theoretical analysis and experimental verification. IEEE Trans. On Microwave Theory and Techniques, MTT-41(12):2376-2382, December 1993

[42] Joseph C. Palais, "Fiber Optic Communications", Pearson Prentice Hall, 2005, page 176-182

[43] C. Cox, E. Ackerman, G. Betts, and J. Prince, "Limits on the performance of RF-over-fiber links and their impact on device design," IEEE Trans. Microwave Theory Tech., vol. 54, no. 2, pp. 906-920, Feb. 2006.

[44] Eduard Sackinger, "Broadband Circuits for Optical Fiber Communication", WILEY & SONS, 2005, page 239-241.

[45] Eduard Sackinger, "Broadband Circuits for Optical Fiber Communication", WILEY & SONS, 2005, page 26-31.